PHYSICAL REVIEW A VOLUME 1, NUMBER 3 MARCH 1970

Spectral Broadening of Elastic Second-Harmonic Light Scattering in Liquids

P. D. Maker
Scientific Research Staff, Ford Motor Company, Dearborn, Michigan 48121
(Received 4 July 1969)

The spectral width of "elastic" second-harmonic light scattering has been measured for a number of liquids. The broadening arises principally from rotational molecular motions and, ignoring possible nonadditive molecule-molecule interactions, the spectrum is shown to be related to the Fourier transform of the orientation-dependent pair distribution function $G(\vec{r}, \vec{\Omega}, t)$. An irreducible spherical-tensor representation is employed. It is shown that a totally symmetric nonlinear-susceptibility tensor produces elastic harmonic light scattering characterized by just the first- and third-degree spherical elements of $G(\vec{r}, \vec{\Omega}, t)$ and that the corresponding spectra may be independently determined. For Brownian orientational motion, these comprise Lorentzians whose widths are related to the tensorial orientational-diffusion coefficient. For isotropic orientational diffusion, the widths are in the ratio 1:6. Dielectric relaxation and depolarized Rayleigh scattering also relate to $G(\vec{r}, \vec{\Omega}, t)$, and the results of all three experiments are compared. In no instance was isotropic orientational diffusion found to be a satisfactory model. A more extended study was made of carbon tetrachloride. Evidence was found both for nonadditive response and for coherent effects resulting from short-range orientational ordering. The extremely weak signals – often less than one photoevent per laser firing – necessitated development of a reliable high-repetition-rate Q-switched ruby laser and use of electronic data-accumulation techniques.

I. INTRODUCTION

An earlier paper[1] described measurements of second-harmonic light scattering. In those experiments, a Q-switched ruby laser was brought to focus within suitable isotropic optical materials, and light whose optical frequency was near twice the laser's was detected coming from the focal region. The paper reported upon the intensity, polarization, and spectrum (with 100-cm^{-1} resolution) of this harmonic light scattering and interpreted the effect in terms of macroscopic material parameters. The spectrum was generally dominated by a strong unresolvable "elastic" peak – the elastic harmonic light scattering (EHLS) – centered exactly at twice the laser frequency. Weak "inelastic" sidebands displaced by molecular vibrational frequencies from the EHLS peak were also found.

The effect had been anticipated[2,3] and has been discussed both macroscopically and microscopically by a number of authors.[4-7] It is ascribable to electric polarization induced by the square of the applied electric field upon the microscopic constituents of an otherwise isotropic medium. For most materials, the responsible nonlinear susceptibility may be described adequately by a real symmetric tensor. In that case, the harmonic light scattering comprises two parts separable by polarization effects. In the completely general case, six components may be distinguished. The EHLS process is coherent, but only by virtue of correlations in the orientation of the scattering elements.

In a fluid, the scatterers are conveniently identified with the constituent molecules. The motions of the molecules, particularly their rotational motions, will time modulate the nonlinear polarization and produce spectral broadening of the EHLS. The broadening produced by rotational motions will be of the order of the reciprocal of the orientational relaxation time (a few cm^{-1}). The data of the earlier paper indicated that at the very high resolution required to detect this broadening, the peak signal would fall to less than one photoelectron per laser firing. By employing a high-repetition-rate laser, a high-dispersion monochromator, and an electronic data-processing system, this broadening has been measured in a number of pure liquids. The essential purpose of this paper is to report and interpret those findings.

In Sec. II the scattering theory is first developed in terms of an orientation-dependent pair correlation function. All angular dependencies are then expanded in spherical harmonics, spherical tensors are introduced, and it is shown that the two (for a totally symmetric susceptibility tensor) distinguishable parts of the unresolved EHLS give rise to different spectra. These are just the time Fourier transforms of the $l=1$ and $l=3$ spherical elements of the correlation function. While spherical tensors are widely used, they are perhaps unfamiliar in the present context. Therefore a detailed ac-

count of their use in the current problem is given in an Appendix. The rather general first treatment is followed by a series of simplifying assumptions, and it is shown that in the limit of incoherent scattering from molecules undergoing diffusional-orientational relaxation, an exact solution for the spectrum can be given in terms of the rotational diffusion tensor. The experiment is described in Sec. III, where the results and related literature data are summarized in Table I. Section IV begins with a discussion of the influence of the intense laser beam and competing nonlinear optical effects upon the intrinsic properties of the samples and upon the results. The relationship between dielectric relaxation, EHLS, and depolarized Rayleigh scattering is then developed. Finally the experimental results for individual molecules are discussed and given tentative interpretation in terms of foregoing considerations.

II. THEORY

In the following, a theory for elastic second-harmonic light scattering from the undistorted individual molecules of a liquid will be developed in the Born approximation and under the assumptions that the molecules are small compared to the wavelength and that the dimensions of the sample are large compared to both the light wavelength and to the extent of order within the liquid. It will include consideration of the interference between the scattering from separate molecules. A full theory would in addition consider aggregates of molecules whose total scattering cross section is not given by the sum of the cross sections of its constituents. In this latter category fall effects of distortions, both mechanical and electronic, of the individual molecules from their free-space configuration due to the environment. Thus, as

TABLE I. Summary of EHLS linewidth data.

Liquid	Temp °C	$\rho = I_{\parallel}/I_{\perp}$	$\Delta\nu_{\frac{1}{2}}$ cm^{-1}	τ_{meas} psec	τ_0 psec	Literature values τ_0 psec	Literature values from measure of psec
Water	25 ±1	8.6 ±0.6	1.2 ±0.1	8.8 ±0.8	17.6±1.6	17.4	τ_{DR}=8.7[a]
	60		2.8 ±0.5	3.8 ±0.7	7.6±1.4	7.0	τ_{DR}=3.5[a]
N,*N*-dimethyl formamide	23	3.5 ±0.3	2.2 ±0.4[b]	5 ±0.1	9.6±1.8	20.6	τ_{DR}=10.3[c]
			6.7 ±0.2[b]	1.5 ±0.5	19±6		
Carbon tetrachloride	2		7.9 ±0.8	1.35 ±0.15	16.2±1.8	0.4	τ_{DR}=0.2[d]
	24	1.83 ±0.11	9.8 ±0.1	1.1 ±0.1	13.0±1.2	1.2,6.6	τ_{DRS}=0.2,1.1[d]
	54	1.80 ±0.15	13.1 ±1.5	0.8 ±0.1	9.8±1.2	120	τ_{DRS}=20[e]
	67		15.2 ±1.5	0.7 ±0.1	8.4±1.2		
Chloroform	23	1.51 ±0.13	4.5 ±0.1[f]	2.4 ±0.5	28±6	11	τ_{DR}=5.4[g]
						35	τ_{DRS}=5.9[h]
Acetonitrile	23	10 ±0.1[i]	1.25 ±0.2	8.6 ±1.4	17.2±2.8	7.6	τ_{DR}=3.8[j]
Diethylether	23	6.4 ±0.5	7.2 ±0.5	1.5 ±0.1	3±.2(?)[k]	4.8	τ_{DR}=2.4[l]
Dichloromethane	23	...	5 ±1.5[f]	2.1 ±0.6			
Methylcyclohexane	23	10.4 ±0.6	2.4 ±0.3	4.4 ±0.5	8.8±1		
2-methylbutane	23	10.8 ±2.5	6.2 ±0.1	1.7 ±0.3	3.4±.5		
2,2,4-trimethyl-pentane	23	4.2 ±0.4	4.5 ±0.6	2.4 ±0.3	29±4(?)[m]		
Methanol	23	5.8 ±0.8	<0.2	> 50	>100	98	τ_{D_R}=48.8[a, n]
n-propanol	23	2.2 ±0.5	<0.1	>100	>200	14,000	τ_{D_R}=7000[o]
Isopropanol	23	4.7 ±0.7	<0.2	> 50	>100	520	τ_{D_R}=260[n]

[a] Reference 30.
[b] From polarized spectra. See text.
[c] Reference 31.
[d] Reference 32.
[e] Reference 33.
[f] Background intensity >0.1 I_{peak}.
[g] Reference 34.
[h] Reference 11.
[i] From Ref. 1.
[j] Reference 35.
[k] Using ρ=9.
[l] Reference 36.
[m] Using ρ=1.5.
[n] Reference 37.
[o] Reference 38.

was done in earlier papers,[1-7] it will be assumed that the scattering arises solely from electronic dipole moments induced, proportional to the square of the applied electric field, upon each undistorted molecule of the medium. This moment will be written

$$p_{ai}(t)=\sum_{\alpha,\beta}\beta_{i\alpha\beta}(\vec{\Omega}_a)E_{\mathrm{loc}\alpha}(\vec{r}_a,t)\times E_{\mathrm{loc}\beta}(\vec{r}_a,t)\,. \tag{1}$$

Here $\vec{p}_a(t)$ is the dipole moment induced on molecule a, whose time-dependent position $\vec{r}_a$ and orientation $\vec{\Omega}_a$ are specified in a space-fixed Cartesian reference frame whose origin, for simplicity, is chosen to be the geometric center of the scattering region. $\vec{\Omega}$ stands for the usual Euler angle set (Ψ,Θ,φ).[8] $\underline{\beta}(\vec{\Omega}_a)$ is the nonlinear polarizability or hyperpolarizability tensor for the undistorted molecule a and is real; in Eq. (1), it depends parametrically upon time through $\vec{\Omega}_a$ and the molecular motions. As will be seen, it is this additional source of time dependence that gives a natural spectral width to the EHLS even though the laser might be perfectly monochromatic. References 9 and 10 summarize existing knowledge of $\underline{\beta}$, and, among others,[11-14] Gordan[15] has investigated the effects of molecular motions on infrared absorption, Raman, and depolarized Rayleigh scattering spectra. $\vec{E}_{\mathrm{loc}}(\vec{r}_a,t)$ is the real vector amplitude of the local electric field and will be assumed to be related to the applied optical frequency electric field $\vec{E}(\vec{r}_a,t)$ through a simple Lorentz factor by

$$\vec{E}_{\mathrm{loc}}(\vec{r}_a,t)=\tfrac{1}{3}(n^2+2)\vec{E}(\vec{r}_a,t)\,, \tag{2}$$

n being the refractive index. The intermolecular field contributes to $\vec{E}_{\mathrm{loc}}$ a time-varying component which is independent of the applied field. In combination with the square of the applied field and the higher-order nonlinear polarizabilities, this intermolecular field can produce frequency-broadened second-harmonic light scattering. Such an effect has been examined theoretically by Keilich[5] and Weinberg[7] and is found to be significant in certain cases. Further discussion of its possible influence upon our experimental results will be postponed to Sec. IV. Equation (1) implies instantaneous response of the molecular system to the applied fields, or that the medium is lossless. This of course is not the case, but this assumption is not critical to the results of the development provided no resonant behavior occurs at frequencies between the laser frequency and its harmonic.

In practice, the laser beam was brought to a rather sharp focus within a large continuous sample. The electric field of the laser will be represented by a plane wave whose amplitude is zero outside of the focal volume, and is constant and equal to an appropriately weighted average over the focal volume of the actual field. Thus,

$$E_i(\vec{r}_a,t)=\mathcal{E}_i\cos(\vec{k}_0\cdot\vec{r}_a-\omega_0 t+\varphi_i)\,, \tag{3}$$

$\vec{\mathcal{E}}$ being the average field amplitude; $\omega_0/2\pi=f_0$, the laser frequency; $|\vec{k}_0|=\omega_0/c$, the magnitude of the wave vector $\vec{k}_0$ which points in the direction of propagation of the laser beam; φ_i, the phase of the ith vector component of $\vec{\mathcal{E}}$; and $c_0=nc$, the vacuum light velocity. Retaining only the Fourier component of $\vec{E}^2(\vec{r},t)$ at twice the laser frequency,

$$p_{ai}(t)=\tfrac{1}{2}[\tfrac{1}{3}(N^2+2)]^2\sum_{\alpha,\beta}\beta_{i\alpha\beta}(\vec{\Omega}_a)\mathcal{E}_\alpha\mathcal{E}_\beta\times\cos(2\vec{k}_0\cdot\vec{r}_a-2\omega_0 t+\varphi_\alpha+\varphi_\beta)\,. \tag{4}$$

At some observation point $\vec{R}$, the electric field $E_{sq}(\vec{R},t)$ of the scattered radiation propagating toward that point and polarized in direction $\vec{q}$ (where $\vec{q}\cdot\vec{R}\equiv 0$) is given in the wave zone ($R\equiv|\vec{R}|\equiv\gg\lambda\equiv c/f_0$) by[16]

$$E_{sq}(\vec{R},t)=\frac{n^2+2}{3}\frac{1}{c_0^{\,2}}\sum_{a=1}^{N}\frac{1}{R_a}\frac{\partial^2}{\partial t^2}p_{aq}\left(t-\frac{R_a}{c}\right), \tag{5}$$

where $\vec{R}_a\equiv\vec{R}-\vec{r}_a$ and N is the number of molecules within the focal volume V_S. Since the average molecular velocity is very small compared to the light velocity, $\vec{R}_a$ in Eq. (5) may be taken at time t. Assuming $R_a\gg V_S^{1/3}$, and inserting (1) and (2), Eq. (5) becomes

$$E_{sq}(\vec{R},t)=-\left(\frac{n^2+2}{3}\right)^3\frac{2\omega_0^{\,2}}{Rc_0^{\,2}}\sum_{\substack{a=1\\ \alpha,\beta}}^{N}\mathcal{E}_\alpha\mathcal{E}_\beta\beta_{q\alpha\beta}(\vec{\Omega}'_a)\times\cos\{2\vec{k}_0\cdot\vec{r}\,'_a-2\omega_0[t-(R_a/c)]\}\,. \tag{6}$$

The primed position and orientation variables signify their values at the retarded time $t-(R_a/c)$, i.e., $\vec{r}\,'_a\equiv\vec{r}_a[t-(R_a/c)]$. Here the time derivatives indicated in (6) have been performed only upon the optical frequency terms since the remaining time-dependent quantities vary much more slowly. The discussion will immediately be restricted to analysis of the plane-polarized scattering. In certain specialized cases, further information can be gained by studying circularly polarized scattering, but no experiments of this

sort were conducted.

Let $I_q(\vec{R},\omega)$ be the intensity per unit frequency interval of the scattered radiation associated with E_{sq}. It is given in terms of the cosine Fourier transform of the space-time correlation function of the total scattered electric field by[17]

$$I_q(\vec{R},\omega)=\frac{nc_0}{4\pi}\int_{-\infty}^{\infty}d\tau\cos\omega\tau \times\langle E_{sq}(\vec{R},t)E_{sq}(\vec{R},t+\tau)\rangle . \quad (7)$$

Here the symbol $\langle\ \ \rangle$ stands for the average over time t, the result being independent of t. Note that $\langle f(-\tau)\rangle=\langle f(\tau)\rangle$ for any $f(\tau)$. Inserting for $\vec{E}_S(\vec{R},t)$,

$$I_q(\vec{R},\omega)=\left(\frac{n^2+2}{3}\right)^6\frac{n\omega_0{}^4}{\pi R^2c_0{}^3}\sum_{\substack{a,b=1\\ \alpha,\beta,\gamma,\delta}}^{N}\mathcal{E}_\alpha\mathcal{E}_\beta\mathcal{E}_\gamma\mathcal{E}_\delta \times\int_{-\infty}^{\infty}d\tau\cos\omega\tau\,\langle\beta_{q\alpha\beta}[\vec{\Omega}'_a(t)]\beta_{q\gamma\delta} \times[\Omega'_b(t+\tau)]\cos\{2\vec{k}_0\cdot[\vec{r}'_b(t+\tau)-\vec{r}'_a(t)] -2\omega_0\left(\tau-\frac{R_b-R_a}{c}\right)-\varphi\}\rangle , \quad (8)$$

where $\varphi\equiv\varphi_\alpha+\varphi_\beta-\varphi_\gamma-\varphi_\delta$. The right-hand side of Eq. (8) should include a sum frequency term. Since the spectrum of molecular motions contains no Fourier components near $4\omega_0 t$, the term will vanish upon performing the time average and has, therefore, been dropped.

The quantity remaining to be time-averaged in (8) depends upon time only parametrically, through its dependence upon the molecular positions and orientations. Thus, invoking the ergodic theorem, the time average may be replaced by an ensemble average,[18] i.e.,

$$\langle F[\vec{r}'_a(t),\vec{r}'_b(t+\tau),\vec{\Omega}'_a(t),\vec{\Omega}'_b(t+\tau)]\rangle = \int_{V_S}d\vec{r}_1\int_{V_S}d\vec{r}_2\int_{8\pi^2}d\vec{\Omega}_2\,F(\vec{r}_1,\vec{r}_2,\vec{\Omega}_1,\vec{\Omega}_2) \times f_J(a:\vec{r}_1,\vec{\Omega}_1,t-R_1/c\,|\,b:\vec{r}_2,\vec{\Omega}_2,t+\tau-R_2/c) , \quad (9)$$

where f_J is the joint probability density of finding molecule a with coordinates $\vec{r}_1,\vec{\Omega}_1$ at time $t-(R_1/c)$ and molecule b with coordinates $\vec{r}_2,\vec{\Omega}_2$ at time $t+\tau-(R_2/c)$. Regarding all molecules as being equivalent upon averaging,

$$\sum_{a,b=1}^{N}f_J=\frac{N}{8\pi^2V_S}\,G(\Delta\vec{r},\Delta\vec{\Omega},\tau+\frac{\vec{R}\cdot\Delta\vec{r}}{Rc}) , \quad (10)$$

where $\Delta\vec{r}\equiv\vec{r}_2-\vec{r}_1$; $\Delta\vec{\Omega}\equiv\vec{\Omega}_2-\vec{\Omega}_1$;

and, since $R_1\equiv[(\vec{R}-\vec{r}_1)\cdot(\vec{R}-\vec{r}_1)]^{1/2}\cong R-\vec{R}\cdot\vec{r}_1/R$,

$$R_2-R_1\cong-\vec{R}\cdot\Delta\vec{r}/R.$$

Here $G(\vec{r},\vec{\Omega},t)$ is van Hove's density-density correlation function[19] generalized to include the orientation coordinates. Thus, $G(\vec{r},\vec{\Omega},t)$ is the probability density of finding a molecule at $\vec{r}$ with orientation $\vec{\Omega}$ at time t after a molecule (the same or any other) was at $\vec{r}\equiv0,\vec{\Omega}\equiv0$. Deriving from time-reversible laws of microscopic motion, the generalized van Hove function will be symmetric under time reversal,[18] i.e.,

$$G(\vec{r},\vec{\Omega},-t)=G(\vec{r},\vec{\Omega},t) . \quad (11)$$

Whereas the usual van Hove function depends only upon $|\vec{r}|$, the present function, as defined, depends also upon the direction of $\vec{r}$ relative to the initial (i.e., $\Omega\equiv0$) orientation of the molecule. Since the particles are indistinguishable, the relation

$$G(-\vec{r},-\vec{\Omega},-t)=G\{D(\vec{\Omega})\vec{r},\vec{\Omega},t\} \quad (12)$$

will hold. Here $D(\vec{\Omega})$ is the operator for a rotation of the reference coordinate frame by amount $\vec{\Omega}$.[20] Further, as no molecular deformations are allowed, in first approximation, $G(\vec{r},\vec{\Omega},t)$ will belong to the same symmetry-point group as the individual molecules, both in $\vec{\Omega}$ and in the angular coordinates of $\vec{r}$.

Using this notion, the intensity (8) becomes

$$I_q(\vec{R},\omega)=\left(\frac{n^2+2}{3}\right)^6\frac{n\omega_0{}^4N}{\pi R^2c_0{}^3}\sum_{\alpha,\beta,\gamma,\delta}\mathcal{E}_\alpha\mathcal{E}_\beta\mathcal{E}_\gamma\mathcal{E}_\delta \times\int_{-\infty}^{\infty}d\tau\cos\omega\tau\int\frac{d\vec{\Omega}}{8\pi^2}\int d\Delta\vec{\Omega}\int d\Delta\vec{r} \times G(\Delta\vec{r},\Delta\vec{\Omega},\tau+\vec{R}\cdot\Delta\vec{r}/cR)\,\beta_{q\alpha\beta}(\vec{\Omega})\beta_{q\gamma\delta}(\vec{\Omega}+\Delta\vec{\Omega}) \times\cos[2\vec{k}_0\cdot\Delta\vec{r}-2\omega_0(\tau+\vec{R}\cdot\Delta\vec{r}/cR)-\varphi] , \quad (13)$$

where, in addition to (10), the substitutions $\vec{r}\equiv\vec{r}_1$ and $\vec{\Omega}\equiv\vec{\Omega}_1$ have been used, and the trivial integration over $\vec{r}$ has been performed.

Next, the third-rank Cartesian tensor $\beta_{ijk}(\vec{\Omega})$ is expanded in spherical representation according to

the relation

$$\beta_{ijk}(\vec{\Omega}) = \sum_{\nu,l,m} \beta_m^{[\nu,l]}(\vec{\Omega})\, c_{ijk}^{\nu lm} \quad . \tag{14}$$

The details of this expansion, including a derivation of the matrix $c_{ijk}^{\nu lm}$, are given in the Appendix. Briefly, in (14), $\beta_m[\nu,l](\vec{\Omega})$ transforms under proper rotations like the mth spherical harmonic of degree l, i.e., like the angular momentum eigenfunction representing a state having total angular momentum $\hbar l$ and z component of angular momentum $\hbar m$. The index ν specifies the symmetry of β_{ijk} upon interchange of its Cartesian subscripts. There are four definable symmetry species under this interchange operation. Only those for which β_{ijk} is invariant upon interchange of j and k are measurable via harmonic light scattering. Two such species exist; one being symmetric on interchange of i and j (to be denoted by $\nu = ss$), the other having undefined or mixed symmetry on interchange of i and j (to be denoted $\nu = ms$). If β_{ijk} is totally symmetric (i.e., $\nu = ss$ only), as is the case when the material is transparent throughout the frequency region $\omega \ll \omega_0$ to $\omega \gg 2\omega_0$, l can assume only the values $l=3$ (for which $-3 \leq m \leq 3$) and $l=1 (-1 \leq m \leq 1)$. For the species $\nu = ms$, l assumes the values one and two. For the sake of generality, the remaining species, although of no practical interest at this time, are treated in the Appendix.

As discussed in the Appendix, the dependence of $\beta_m[\nu,l](\vec{\Omega})$ upon the molecular orientation $\vec{\Omega}$ can be given[20] explicitly as the contraction of the finite rotation matrix $D_{km}^{(l)}(\vec{\Omega})$ with $\bar{\beta}_m[\nu,l]$, the property tensor expressed in a molecular fixed coordinate frame, i.e.,

$$\beta_m^{[\nu,l]}(\vec{\Omega}) = \sum_{k=-l}^{l} D_{mk}^{[l]}(\vec{\Omega})\, \bar{\beta}_k^{[\nu,l]} \quad . \tag{15}$$

The superscript $(\bar{\ })$ is introduced to distinguish tensor properties referred to molecular fixed coordinate frames. Inserting (14) and (15) into (13) and, for later convenience, using the presumed reality of β_{ijk} [both $c_{ijk}^{\nu lm}$ and $\beta_m[\nu,l](\vec{\Omega})$ are complex quantities], one obtains

$$I_q(R,\omega) = \left(\frac{n^2+2}{3}\right)^6 \frac{n\omega_0^4 N}{\pi R^2 c_0^3} \sum_{\substack{\alpha,\beta,\gamma,\delta \\ \nu,\nu',l,l' \\ m,m',k,k'}} \mathcal{E}_\alpha \mathcal{E}_\beta \mathcal{E}_\gamma \mathcal{E}_\delta\, c_{q\alpha\beta}^{\nu lm}\, c_{q\gamma\delta}^{\nu' l' m'*}$$

$$\times \bar{\beta}_k^{[\nu,l]} \bar{\beta}_{k'}^{[\nu',l']*} \int_{-\infty}^{\infty} d\tau \int d(\Delta\vec{\Omega}) \int d(\Delta\vec{r}) \int \frac{d\vec{\Omega}}{8\pi^2} D_{mk}^{[l]}(\vec{\Omega})\, D_{m'k'}^{[l']*}(\vec{\Omega}+\Delta\vec{\Omega})$$

$$\times \cos\omega\tau\, G\left(\Delta\vec{r}, \Delta\vec{\Omega}, \tau + \frac{\vec{R}\cdot\Delta\vec{r}}{cR}\right) \cos\left[2\vec{k}_0\cdot\Delta\vec{r} - 2\omega_0\left(\tau + \frac{\vec{R}\cdot\Delta\vec{r}}{cR}\right) - \varphi\right] \quad . \tag{16}$$

Using various of the properties of the $D_{km}^{[l]}(\vec{\Omega})$ functions, as given in (A24) of the Appendix, the integral over $\vec{\Omega}$ reduces to

$$\int (\cdots) \frac{d\vec{\Omega}}{8\pi^2} = \frac{\delta_{ll'}\delta_{mm'}}{2l+1} D_{kk'}^{[l]*}(\Delta\vec{\Omega}) \quad . \tag{17}$$

Let us perform a Fourier expansion of $G(\vec{r}, \vec{\Omega}, t)$ in $\vec{r}$ and t and expand its dependence upon $\vec{\Omega}$ in terms of the complete set $D_{km}^{[l]}(\vec{\Omega})$, so that

$$G(\vec{r},\vec{\Omega},t) = \frac{1}{(2\pi)^4} \frac{2l+1}{8\pi^2} \int_{-\infty}^{\infty} d\vec{k} \int_{-\infty}^{\infty} d\omega\, e^{i(\vec{k}\cdot\vec{r} - \omega t)}$$

$$\times \sum_{l,k,m} D_{km}^{[l]}(\vec{\Omega})\, G_{km}^{[l]}(\vec{k},\omega) \quad . \tag{18}$$

The inverse transform takes the form

$$G_{km}^{[l]}(\vec{k},\omega) = \int_{8\pi^2} d\vec{\Omega} \int_{-\infty}^{\infty} d\vec{r} \int_{-\infty}^{\infty} dt\, e^{-i(\vec{k}\cdot\vec{r} - \omega t)}$$

$$\times D_{km}^{[l]*}(\vec{\Omega}) G(\vec{r},\vec{\Omega},t) \quad . \tag{19}$$

Since $G(\vec{r},\vec{\Omega},t) = G(\vec{r},\vec{\Omega},-t)$, $G_{km}{}^{l}(\vec{k},\omega) = G_{km}{}^{l} \times (\vec{k},\omega)$. As a function of $\vec{r}$, $G(\vec{r},\vec{\Omega},t)$ becomes constant, equal to its continuum value $N/8\pi^2 V_S$, for distances $\vec{r}$ larger than a few times the phonon damping length. In the phonon frequency range being dealt with, this length is small compared to the dimensions of the scattering volume, so that the integrals over $\vec{r}$ in Eqs. (9), (3), and (16) may safely be extended to infinity. Thus, on inserting (17) and (18) into (16) and performing the integrations, we obtain

$$I_q(\vec{R},\omega) = \left(\frac{n^2+2}{3}\right)^6 \frac{n\omega_0^4 N}{4\pi R^2 c_0^3} \sum_{\substack{\alpha,\beta,\gamma,\delta \\ \nu,\nu' l,m,k,k'}} \mathcal{E}_\alpha \mathcal{E}_\beta \mathcal{E}_\gamma \mathcal{E}_\delta$$

$$\times c_{q\alpha\beta}^{\nu lm} c_{q\gamma\delta}^{\nu' lm *} \frac{\bar{\beta}_k^{[\nu,l]} \bar{\beta}_{k'}^{[\nu',l]*}}{2l+1}$$

$$\times \{ G_{kk'}^{[l]}(\Delta k, \Delta\omega) e^{-i\varphi}$$

$$+ G_{kk'}^{[l]}(-\Delta\vec{k}, \Delta\omega) e^{i\varphi} \} , \qquad (20)$$

where $\Delta\omega \equiv \omega - 2\omega_0$ is the frequency shift and $\Delta\vec{k} = \vec{k}_S - 2\vec{k}_0 = (\omega/c)(\vec{R}/R) - 2\vec{k}_0$ is the wave vector shift upon scattering.

Equation (20) is a quite general expression for the intensity of EHLS in terms of fundamental properties of the scattering system, i.e., the molecular property tensor $\bar{\beta}_m^{[\nu,l]}$ and the system pair correlation function. Its generality is limited chiefly by the assumption that the bulk properties may adequately be expressed in terms of the properties of individual undistorted molecules. Other assumptions involved in the derivation are apt to be very realistic for the considered experiment applied to a wide range of liquids and gases. Note that the density fluctuations which give rise to Brillouin scattering are an isotropic material property and are contained in the orientation-independent pair correlation function $G(\vec{r}, t)$ defined by

$$G(\vec{r}, t) = \int d\vec{\Omega}\, G(\vec{r}, \vec{\Omega}, t) . \qquad (21)$$

From (19), we see that $G(\vec{r}, t) \equiv G_{00}^{[0]}(\vec{r}, t)$. Since $\bar{\beta}_k^{[\nu,l]}|_{l=0}$ makes no contribution to EHLS, density fluctuations will not be observed.

It should be noted that the intensity of the Rayleigh scattering may be expressed in a form identical to that of Eq. (20), $\bar{\alpha}_m^{[\nu,l]}$ and $c_{q\alpha}^{\nu lm}$ replacing $c_{q\alpha\beta}^{\nu lm}$ and $\bar{\beta}_m^{[\nu,l]}$. As $\bar{\bar{\alpha}}$ contains spherical components having $l = 0$, 1, and 2, information is available, in principle, concerning the various spherical expansion coefficients of the orientation-dependent pair correlation function for l out to 3, with, in fact, several cross checks. Dielectric relaxation also relates, indirectly, to the $l = 1$ elements of $G_{km}^{[l]}(\vec{k}, \omega)$, the connection involving macroscopic and induced polarization effects.[13,21,22] NMR line broadening in certain instances relates, again indirectly, to the $l = 2$ elements of $G_{km}^{[l]}(\vec{k}, \omega)$.[23,24] These interrelations will be discussed further in Sec. IV.

A series of simplifying assumptions, progressively more restrictive, will now be introduced so as to reduce (20) to a form more suited for comparison with the available data. First, note that the orientational ordering found in liquids will most often be of rather short range. If it extends to distances short compared to $1/|\Delta\vec{k}|$ (300 Å for the present experiments), the factor $e^{-i\Delta\vec{k}\cdot\vec{r}}$ appearing in Eq. (19) may set equal to unity. $G_{km}^{[l]}(\Delta\vec{k}, \omega)$ is then independent of $\Delta\vec{k}$ and is just the Fourier-transformed spherical expansion coefficient of $\int_{-\infty}^{\infty} d\vec{r}^{\,3}\, G(\vec{r}, \vec{\Omega}, t)$, i.e., of the total probability density of finding some molecule with orientation $\vec{\Omega}$ a time t after a test molecule had orientation $\vec{\Omega} = 0$, independent of their relative separation. Equation (20) then becomes

$$I_q(\vec{R}, \omega) = \left(\frac{n^2+2}{3}\right) \frac{n\omega_0^4 N}{4\pi R^2 c_0^3} \sum_{\substack{\alpha,\beta,\gamma,\delta \\ \nu,\nu',l,m,k,k'}}$$

$$\times \mathcal{E}_\alpha \mathcal{E}_\beta \mathcal{E}_\gamma \mathcal{E}_\delta\, c_{q\alpha\beta}^{\nu lm} c_{q\gamma\delta}^{\nu' lm *}$$

$$\times \frac{\bar{\beta}_k^{[\nu,l]} \bar{\beta}_{k'}^{[\nu',l]*}}{2l+1} G_{kk'}^{[l]}(\Delta\omega) \cos\varphi . \qquad (22)$$

Second, as discussed in the Appendix, to good approximation $\bar{\beta}$ may be assumed to be a totally symmetric tensor, i.e., $\bar{\beta}_k^{[\nu,l]}$ may be set equal to zero unless $\nu = ss$. In that case, l may assume only the values one and three, the indices ν and ν' may be suppressed, and we observe that the EHLS spectrum consists in fact of two separate parts:

$$\sum_{k,k'} \bar{\beta}_k^{[l]} \bar{\beta}_{k'}^{[l]*} G_{kk'}^{[l]}(\Delta\omega),$$

$$\text{for } l = 1 \quad \text{and } l = 3 . \qquad (23)$$

These two spectra will henceforth be denoted as the $\bar{\beta}^{[1]}$ and $\bar{\beta}^{[3]}$ spectra. As will be shown in a later paper, a similar result holds for inelastic harmonic light scattering; further, the $\bar{\beta}^{[1]}$ spectrum obeys "dipole" selection rules, as does the infrared absorption spectrum. The $\bar{\beta}^{[3]}$ spectrum, however, obeys "octapole" selection rules and permits observation of a new class of molecular excitations.[4] It will shortly be demonstrated that these two spectra may be measured independently.

Next, decompose $G(\vec{\Omega}, t)$ via the relation

$$G(\vec{\Omega}, t) = G_s(\vec{\Omega}, t) + G_d(\vec{\Omega}, t) . \qquad (24)$$

Here $G_s(\vec{\Omega}, t)$ is the self-correlation function (the probability density that the test molecule itself has orientation $\vec{\Omega}$ a time t after it was at $\vec{\Omega} = 0$) while $G_d(\vec{\Omega}, t)$ is the "different molecule" correlation function. No detailed knowledge of $G_d(\vec{\Omega}, t)$ exists, and its actual importance in the present context, as will be seen in the discussion of Sec. IV,

is not at all clear. Little can be done with the term except that, if the local environment about the test molecule is assumed to remain constant as that molecule wanders, then

$$G_{km}^{[l]}(\omega)=\sum_{m'} G_{s\,km'}^{[l]}(\omega)N_{m'm}^{[l]}, \tag{25}$$

where $N_{m'm}^{[l]}$, defined by

$$N_{m'm}^{[l]}=\delta_{m'm}+G_{dm'm}^{[l]}, \tag{26}$$

is the total number of molecules, weighted appropriately by their orientation, correlated about the test molecule. $G_{dm'm}^{[l]}$ are the spherical expansion coefficients of $G_d(\vec{\Omega})$.

The orientational self-correlation function $G_s(\vec{\Omega},t)=\int_{-\infty}^{\infty} d\vec{r}\, G_s(\vec{r},\Omega,t)$ can be determined if $\kappa(\vec{\Omega})$, the probability density per unit time that a molecule will undergo a change of orientation by amount $\vec{\Omega}$ is known.[21,25] Expanding the continuity equation

$$\frac{\partial}{\partial t}G_s(\vec{\Omega},t)=\int_{8\pi^2} d\vec{\Omega}'\, G_s(\vec{\Omega}-\vec{\Omega}',t)\kappa(\vec{\Omega}')-G_s(\vec{\Omega},t)\times\int_{8\pi^2} d\vec{\Omega}'\kappa(\vec{\Omega}') \tag{27}$$

in the $D_{km}^{[l]}(\vec{\Omega})$ functions, the following set of coupled linear differential equations results:

$$\frac{\partial}{\partial t}G_{s\,km}^{[l]}(t)=\sum_{m'} G_{s\,km'}^{[l]}(t)\times[\kappa_{m'm}^{[l]}-\kappa_{00}^{[l]}\delta_{m'm}]. \tag{28}$$

The set may be solved readily by Laplace transforms. The spherical elements of $G_s(\vec{\Omega},t)$ on this model are seen to decay exponentially, the time constants for a particular element depending upon some combination of the spherical expansion coefficients of $\kappa(\vec{\Omega})$.

In a consummate attempt to reduce (20) and relate the EHLS spectral broadening to more common experience, assume that $G_s(\vec{r},\vec{\Omega},t)$ results from thermally activated Brownian motion. The dependence of G_s upon $\vec{r}$ will be reintroduced as a time-dependent factor, and it will be seen that even this consideration is unimportant to the EHLS. Thus, if $G_s(\vec{r},\vec{\Omega},t)=g_r(\vec{r},t)g_\Omega(\vec{\Omega},t)$, then the g's represent solutions to simple diffusion equations of the form[24-27]

$$\left(\frac{\partial}{\partial t}-D_\Omega\nabla_\Omega^2\right)g_\Omega(\vec{\Omega},t)=0, \tag{29}$$

$$\left(\frac{\partial}{\partial t}-D_r\nabla_r^2\right)g_r(|\vec{r}|,t)=0, \tag{30}$$

where D_r is the translational diffusion coefficient, D_Ω is the (here assumed scalar) rotational diffusion coefficient and ∇_r^2 and ∇_Ω^2 the Laplacians in position and orientation[27,28] space. The diffusion coefficients are given in terms of the viscous drag resisting the motions, B, by $D=kT/B$, and going still further to the Debye-Stokes limit,[24,26]

$$B_\Omega=8\pi a^3\eta=\tfrac{4}{3}a^2B_r. \tag{31}$$

In this approximation, the molecules are assumed to be small spheres of radius a moving classically in a continuum having viscosity η. A real liquid might thus have $D_\Omega=10^{11}$ sec^{-1} and $D_r=10^{-5}$ sec^{-1} cm^{-2}.

Subject to the initial values

$$g_r(\vec{r},0)=\delta(\vec{r}), \tag{32}$$

$$g_\Omega(\vec{\Omega},0)=\delta(\vec{\Omega}),$$

where $\delta(x)$ is the Dirac δ function, (29) and (30) have the classical solutions[24-27]

$$g_\Omega(\vec{\Omega},t)=\sum_{l=0}^{\infty}\sum_{k=-l}^{l}\frac{2l+1}{8\pi^2}D_{kk}^{[l]}(\vec{\Omega})e^{-|t|/\tau_{lk}}, \tag{33}$$

$$g_r(\vec{r},t)=(4\pi D_r|t|)^{-3/2}\exp(-r^2/4D_r|t|),$$

$$\text{with}\quad 1/\tau_{lk}=1/\tau_l=l(l+1)D_\Omega. \tag{34}$$

For nonspherical molecules, the rotational diffusion coefficients become tensors.[26,27] If an axis of symmetry (threefold or higher) remains, the rotational diffusion Eq. (29) has the solution (33), but with

$$1/\tau_{lk}=l(l+1)D_{\Omega,z}+k^2(D_{\Omega,xy}-D_{\Omega,z}), \tag{35}$$

where $D_{\Omega,z}$ is the diffusion coefficient for rotations about the figure axis and $D_{\Omega,xy}$ is for rotations about axes in the xy plane. No closed solution of the form (33) exists for rotational diffusion of an anisotropic molecule. The relaxation times in that case involve three diffusion coefficients, one for rotation about each principal axis. The problem is in direct analogy to that of determining the energy levels of an asymmetric rotor and has been treated in full detail by Favro.[26] Since all

dependence upon the translation diffusion is shortly to be dropped, we need not be concerned with the tensor nature of D_γ.

Using this solution for $G_S(\vec{r}, \vec{\Omega}, t)$ and Eq. (25) to define $G(\vec{r}, \vec{\Omega}, t)$ (i.e., a simple model for the correlations is adopted), we find that according to Eq. (19),

$$G_{s\,k'k}^{[l]}(k, \omega) = \delta_{kk'} \frac{2\tau_{r,l}}{1+\omega^2\tau_{r,l}^2} \ , \tag{36}$$

where $1/\tau_{r,l} = (1/\tau_l) + (1/\tau_r) = l(l+1)D_\Omega + 4|\vec{k}|^2 D_r$. (37)

Using the Debye-Stokes approximation to D_Ω and D_γ, $1/\tau_l \gg 1/\tau_\gamma = 4|\vec{k}|^2 D_\gamma$, i.e., the contribution to the scattering of the translational motion is indeed negligible. Setting $1/\tau_\gamma = 0$, the scattered intensity becomes

$$I_q(\vec{R}, \omega) = \left(\frac{n^2+2}{3}\right)^6 \frac{n\omega_0^4 N}{4\pi R^2 c_0^3} \sum_{\substack{\alpha,\beta,\gamma,\delta \\ \nu,\nu',l,m,k,k'}} \times \mathcal{E}_\alpha \mathcal{E}_\beta \mathcal{E}_\gamma \mathcal{E}_\delta c_{q\alpha\beta}^{\nu lm} c_{q\gamma\delta}^{\nu' lm*} \times \frac{N_{kk'}^{[l]} \overline{\beta}_k^{[\nu' l]} \overline{\beta}_{k'}^{[\nu', l]*}}{2l+1} g_l(\Delta\omega)\cos\varphi \ , \tag{38}$$

where the line-shape function $g_l(\Delta\omega)$ is given by

$$g_l(\Delta\omega) = 2\tau_l/[1+(\tau_l\,\Delta\omega)^2] \ . \tag{39}$$

The spectrum of the EHLS with these approximations is comprised of a series of Lorentzians centered at $\Delta\omega = 0$, one for each allowed value of l whose full width at half-maximum (FWHM) is $l(l+1)D_\Omega$.

For isotropic rotational diffusion let us use Table II of the Appendix to make explicit the dependence of $I_q(\vec{R}, \omega)$ upon the polarization state of the laser and the relative direction of $\vec{q}$ and $\vec{\mathcal{E}}$. With $\mathcal{E}_x = \mathcal{E}\cos\theta$, $\mathcal{E}_y = \mathcal{E}\sin\theta$, $\mathcal{E}_z = 0$, $\varphi_x = 0$, $\varphi_y = \varphi$, and including both the symmetry species $\nu = ss$ and $\nu = ms$, we obtain

$$K^{-1} I_x(R, \omega) = g_1(\Delta\omega)\,\tfrac{1}{45}\,(9\cos^4\theta + \sin^4\theta + 4\cos^2\theta\sin^2\theta + 6\cos^2\theta\cos 2\varphi)\,|\overline{\beta}^{[ss,1]}|^2$$
$$+ (2/9\sqrt{5})\sin^2\theta(1 - 6\cos^2\theta\sin^2\varphi)\,\mathrm{Re}(\overline{\beta}^{[ss,1]}(\overline{\beta}^{[ms,1]*})$$
$$+ (4/3\sqrt{5})\sin^2\theta\cos^2\theta\sin\varphi\cos\varphi\,\mathrm{Im}\,(\overline{\beta}^{[ss,1]}\overline{\beta}^{[ms,1]*}) + \tfrac{1}{9}\sin^2\theta\,|\overline{\beta}^{[ms,1]}|^2]$$
$$+ \tfrac{1}{15} g_2(\Delta\omega)\sin^2\theta\,|\overline{\beta}^{[ms,2]}|^2 + \tfrac{2}{205}\, g_3(\Delta\omega)\,(2 + \cos^2\theta + 6\cos^2\theta\sin^2\theta\sin^2\varphi)\,|\overline{\beta}^{[ss,3]}|^2 \ , \tag{40}$$

$$K^{-1} I_z(\vec{R}, \omega) = g_1(\Delta\omega)\,[\tfrac{1}{45}\,(1 - \sin^2 2\theta\sin^2\varphi)\,|\overline{\beta}^{[ss,1]}|^2 + (2/9\sqrt{5})(1 - \sin^2 2\theta\sin^2\varphi)$$
$$\times \mathrm{Re}(\overline{\beta}^{[ss,1]}\overline{\beta}^{[ms,1]*}) + \tfrac{1}{9}(1 - \sin^2 2\theta\sin^2\varphi)\,|\overline{\beta}^{[ms,1]}|^2]$$
$$+ \tfrac{1}{15}\, g_2(\Delta\omega)(1 + \sin^2 2\theta\sin^2\varphi)\,|\overline{\beta}^{[ms,2]}|^2 + \tfrac{1}{105}\, g_3(\Delta\omega)(4 + \sin^2 2\theta\sin^2\varphi)\,|\overline{\beta}^{[ss,3]}|^2 \ , \tag{41}$$

where $K \equiv [\tfrac{1}{3}(n^2+2)]^6 (n\omega_0^4 N \mathcal{E}^4/4\pi R^2 c_0^3)$. (42)

Equations (40) and (41), apart from the restrictions imposed by the conditions $\vec{q}\cdot\vec{R} = 0$, are independent of the angle between the incident laser beam and the direction of propagation of the scattered radiation. They involve seven material parameters – the rotational diffusion coefficient which determines the line-shape function $g_l(\Delta\omega)$, and six intensity parameters $|\overline{\beta}[ss,1]|^2$, $|\overline{\beta}[ss,3]|^2$, $|\overline{\beta}[ms,1]|^2$, $\mathrm{Re}(\overline{\beta}[ss,1]\overline{\beta}[ms,1]^*)$, $\mathrm{Im}(\overline{\beta}[ss,1]\overline{\beta}[ms,1]^*)$, and $|\overline{\beta}[ms,2]|^2$. Here we have

$$\overline{\beta}[\nu,l]\overline{\beta}[\nu',l]^* \equiv \sum_{\substack{m,m'=-l \\ \text{only}}}^{l} N_{mm'}^{[l]} \overline{\beta}_m^{[\nu,l]} \overline{\beta}_{m'}^{[\nu',l]*} \ . \tag{43}$$

TABLE II. Elements of the unitary tensor $c_{ijk}^{\nu lm}$. The Cartesian and spherical components of the nonlinear susceptibility tensor $\vec{\vec{\beta}}$ are related by $\beta_{ijk} = \sum_{\nu lm} \beta_m^{[\nu,l]} \times c_{ijk}^{\nu lm}$, or inversely by $\beta_m^{[\nu,l]} = \sum_{ijk} c_{ijk}^{\nu lm *} \beta_{ijk}$.

	ijk	zzz	xxz	xzx	zxx	yyz	yzy	zyy	xyz	xzy	zxy	yxz	yzx	zyx
ν	l m													
ss_1	1 0	$-i\sqrt{3/5}$	$-i/\sqrt{15}$	$-i/\sqrt{15}$	$-i/\sqrt{15}$	$-i/\sqrt{15}$	$-i/\sqrt{15}$	$-i/\sqrt{15}$						
ss_3	3 0	$-i\sqrt{2/5}$	$-i/\sqrt{10}$	$-i/\sqrt{10}$	$-i/\sqrt{10}$	$-i/\sqrt{10}$	$-i/\sqrt{10}$	$-i/\sqrt{10}$						
ss_3	3 ± 2		$i/\sqrt{12}$	$i/\sqrt{12}$	$i/\sqrt{12}$	$-i/\sqrt{12}$	$-i/\sqrt{12}$	$-i/\sqrt{12}$	$\pm 1/\sqrt{12}$	$\pm 1/\sqrt{12}$	$\pm 1/\sqrt{12}$	$\pm 1/\sqrt{12}$	$\pm 1/\sqrt{12}$	$\pm 1/\sqrt{12}$
ms_1	1 0		$i/\sqrt{12}$	$i/\sqrt{12}$	$-i/\sqrt{3}$	$i/\sqrt{12}$	$i/\sqrt{12}$	$-i/\sqrt{3}$						
ms_2	2 0								$-1/2$	$-1/2$		$1/2$	$1/2$	
ms_2	2 ± 2		$\mp i/\sqrt{24}$	$\mp i/\sqrt{24}$	$\pm i/\sqrt{6}$	$\pm i/\sqrt{24}$	$\pm i/\sqrt{24}$	$\mp i/\sqrt{6}$	$-1/\sqrt{24}$	$-1/\sqrt{24}$	$1/\sqrt{6}$	$-1/\sqrt{24}$	$-1/\sqrt{24}$	$1/\sqrt{6}$
ma_1	1 0		$i/2$	$-i/2$		$i/2$	$-i/2$							
ma_2	2 0								$1/\sqrt{12}$	$-1/\sqrt{12}$	$-1/\sqrt{3}$	$-1/\sqrt{12}$	$1/\sqrt{12}$	$1/\sqrt{3}$
ma_2	2 ± 2		$\mp i/\sqrt{8}$	$\pm i/\sqrt{8}$		$\pm i/\sqrt{8}$	$\mp i/\sqrt{8}$		$-1/\sqrt{8}$	$1/\sqrt{8}$		$-1/\sqrt{8}$	$1/\sqrt{8}$	
aa	0 0								$1/\sqrt{6}$	$-1/\sqrt{6}$	$1/\sqrt{6}$	$-1/\sqrt{6}$	$1/\sqrt{6}$	$-1/\sqrt{6}$

	ijk	xxx	yyy	xxy	xyx	yxx	yyx	yxy	xyy	zzx	zxz	xzz	zzy	zyz	yzz
ν	l m														
ss_1	1 ± 1	$\pm i\sqrt{3/10}$	$1\sqrt{3/10}$	$1/\sqrt{30}$	$1/\sqrt{30}$	$1/\sqrt{30}$	$\pm i/\sqrt{30}$	$\pm i/\sqrt{30}$	$\pm i/\sqrt{30}$	$\pm i/\sqrt{30}$	$\pm i/\sqrt{30}$	$\pm i/\sqrt{30}$	$1/\sqrt{30}$	$1/\sqrt{30}$	$1/\sqrt{30}$
ss_2	3 ± 1	$\pm i\sqrt{3/40}$	$1\sqrt{3/40}$	$1/\sqrt{120}$	$1/\sqrt{120}$	$1/\sqrt{120}$	$\pm i/\sqrt{120}$	$\pm i/\sqrt{120}$	$\pm i/\sqrt{120}$	$\mp i\sqrt{2/15}$	$\mp i\sqrt{2/15}$	$\mp i\sqrt{2/15}$	$-1\sqrt{2/15}$	$-1\sqrt{2/15}$	$-1\sqrt{2/15}$
ss_3	3 ± 3	$\mp i/\sqrt{8}$	$1/\sqrt{8}$	$-1/\sqrt{8}$	$-1/\sqrt{8}$	$-1/\sqrt{8}$	$\pm i/\sqrt{8}$	$\pm i/\sqrt{8}$	$\pm i/\sqrt{8}$						
ms_1	1 ± 1			$-1/\sqrt{24}$	$-1/\sqrt{24}$	$1/\sqrt{6}$	$\mp i/\sqrt{24}$	$\mp i/\sqrt{24}$	$\pm i/\sqrt{6}$	$\mp i/\sqrt{24}$	$\mp i/\sqrt{24}$	$\pm i/\sqrt{6}$	$-1/\sqrt{24}$	$-1/\sqrt{24}$	$1/\sqrt{6}$
ms_2	2 ± 1			$\pm 1/\sqrt{24}$	$\pm 1/\sqrt{24}$	$\mp 1/\sqrt{6}$	$+i/\sqrt{24}$	$+i/\sqrt{24}$	$-i/\sqrt{6}$	$-i/\sqrt{24}$	$-i/\sqrt{24}$	$+i/\sqrt{6}$	$\mp 1/\sqrt{24}$	$\mp 1/\sqrt{24}$	$\pm 1/\sqrt{6}$
ma_1	1 ± 1			$-i/\sqrt{8}$	$i/\sqrt{8}$		$\pm 1/\sqrt{8}$	$\mp 1/\sqrt{8}$		$\pm 1/\sqrt{8}$	$\mp 1/\sqrt{8}$		$-i/\sqrt{8}$	$i/\sqrt{8}$	
ma_2	2 ± 1			$\mp 1/\sqrt{8}$	$\pm 1/\sqrt{8}$		$-i/\sqrt{8}$	$i/\sqrt{8}$		$-i/\sqrt{8}$	$+i/\sqrt{8}$		$\mp 1/\sqrt{8}$	$\pm 1/\sqrt{8}$	

As shown in Ref. 1, the unresolved EHLS from a macroscopically isotropic medium can always be fully characterized by six intensity parameters. The above expressions relate those parameters to molecular constants. However, if β_{ijk} is real (as has been assumed), it is apparent from Table II of the Appendix that $\bar{\beta}[ss,1]\bar{\beta}[ms,1]^*$ is also real, so that only five of the intensity parameters remain. The formalism can easily be expanded to include complex $\bar{\beta}_{ijk}$, with the result that all six occur. Note also that $\mathrm{Im}(\bar{\beta}[ss,1]\bar{\beta}[ms,1]^*)$ makes no contribution to the plane-polarized scattering when the laser is either plane polarized or elliptically polarized having $\varphi = 90°$, and is the only constant whose contribution is sensitive to the sign of φ. It can readily be seen that if $\bar{\beta}_{ijk}$ is real, $I_q(\vec{R},\Delta\omega)$ must be independent of the sign of φ. One may, by measuring the integrated scattered intensity for several carefully chosen values of θ and φ, determine each of the six intensity parameters listed above. As discussed, to good approximation $\bar{\beta}_m[ms,l]$ may be set equal to zero. Specializing (40) and (41) to this case, dropping the superscript ν and expanding for the geometries of actual experimental interest, the following results are obtained: For a laser beam plane polarized in the x direction, remembering that $\vec{q}\cdot\vec{R} \equiv 0$, we obtain

$$\begin{aligned} K^{-1}I_x(\vec{R},\omega) &= \tfrac{1}{5}g_1(\Delta\omega)\left|\bar{\beta}^{[1]}\right|^2 \\ &\quad + \tfrac{2}{35}g_3(\Delta\omega)\left|\bar{\beta}^{[3]}\right|^2 , \\ K^{-1}I_y(\vec{R},\omega) &= K^{-1}I_z(\vec{R},\omega) = \tfrac{1}{45}g_1(\Delta\omega) \\ &\quad \times\left|\bar{\beta}^{[1]}\right|^2 + \tfrac{4}{105}g_3(\Delta\omega)\left|\bar{\beta}^{[3]}\right|^2 ; \end{aligned} \tag{44}$$

while for circular polarization, $\mathcal{E}_x = \mathcal{E}_y = (1/\sqrt{2})\mathcal{E}$, $\varphi = 90°$,

$$\begin{aligned} K^{-1}I_x(\vec{R},\omega) &= K^{-1}I_y(\vec{R},\omega) = \tfrac{2}{45}g_1(\Delta\omega) \\ &\quad \times\left|\bar{\beta}^{[1]}\right|^2 + \tfrac{8}{105}g_3(\Delta\omega)\left|\bar{\beta}^{[3]}\right|^2 , \\ K^{-1}I_z(\vec{R},\omega) &= \tfrac{1}{21}g_3(\Delta\omega)\left|\bar{\beta}^{[3]}\right|^2 . \end{aligned} \tag{45}$$

The quantity $I_x(\vec{R},\omega)/I_z(\vec{R},\omega) \equiv \rho(\omega)$ will be referred to later as the EHLS "polarization ratio." Unless it is stated that a circularly polarized laser (having $\mathcal{E}_x = \mathcal{E}_y$) is employed, it will be understood when discussing $\rho(\omega)$ that the laser is plane polarized in the x direction.

Equations (44) and (45) will serve as a starting point for the discussion of the data. In this approximation, the EHLS spectrum consists of at the most two Lorentzians whose FWHM's are $2D_\Omega$ and $12D_\Omega$ and whose heights are proportional to $|\bar{\beta}^{[1]}|^2$ and $|\bar{\beta}^{[3]}|^2$, respectively. Only these three material parameters enter.

When anisotropic rotational diffusion occurs, the results (44) and (45) can be generalized in accordance with the discussion following (34). The procedure is straightforward when an axis of symmetry is present. Several additional parameters are required to characterize the spectrum, however, since the individual k components of $\bar{\beta}_k[l]$ produce lines of different half-widths, as given by (35). The construction of $l=1$ and $l=3$ spectra from $I_x(\vec{R},\omega)$ and $I_z(\vec{R},\omega)$ is still possible. The $l=1$ spectrum would in general contain two Lorentzian components, but with a symmetry axis present, $\bar{\beta}_{\pm 1}[l] = 0$ and a single component whose width is given by $2D_{\Omega,z}$ is measured. The $l=3$ spectrum, even with an axis present, will consist of more than one Lorentzian component, the constants $D_{\Omega,z}$, $D_{\Omega,xy}$, $\sum_{m'} \bar{\beta}_m[l]\bar{\beta}_{m'}[l]^* N_{mm'}[l]$ entering. For completely anisotropic rotational diffusion, still further complexities arise.

By the last relation given in (45), the spectrum of the perpendicularly polarized scattering when circularly polarized laser light is used gives directly the line-shape function $g_3(\Delta\omega)$, provided of course that $|\bar{\beta}^{[3]}|^2 \neq 0$. One can then form linear combinations of the other relations (44) and (45) and experimentally, whenever $|\bar{\beta}^{[1]}|^2 \simeq |\bar{\beta}^{[3]}|^2$ determine $g_1(\Delta\omega)$. A check of the applicability of the orientational diffusion model is then provided by comparison of the widths of $g_1(\Delta\omega)$ and $g_3(\Delta\omega)$, which on that theory ought to be in the ratio 1:6. However, the separation of the EHLS spectrum into $\bar{\beta}^{[1]}$ and $\bar{\beta}^{[3]}$ spectra is completely independent of any assumptions on $G(\vec{\Omega},t)$.

III. EXPERIMENT

A. Apparatus

Figure 1 is a schematic diagram of the experimental apparatus. The laser head, a modified Raytheon LH8 unit, was watercooled and employed an FX-47b-6.5 EG&G linear flashtube and a development grade $6\frac{1}{2}$-in.-long by $\frac{3}{8}$-in.-diam 60° Linde Czochralski grown ruby in flat-flat uncoated configuration. The Tyman-Green pattern of the rod showed approximately three fringes. Teflon O-rings, which replaced the original rubber ones at the water seal to the ruby rod, were found to be undamaged by exposure to the lamp flash and, of more importance, caused no significant contamination of the ruby surface at the contact point. Q switching was accomplished via a TIR prism, placed some 150 cm from the end of the ruby, and rotated at about 120 cps. The output-end reflector comprised two fused-quartz optical plane parallels 1.5 and 5

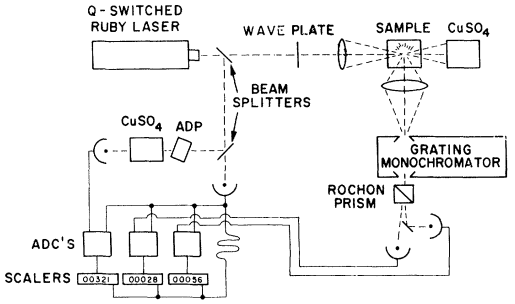

FIG. 1. Experimental apparatus for measuring the spectral profile of elastic second-harmonic light scattering.

mm thick, optically contacted to opposite ends of a plane-parallel Alumalox cylindrical spacer 2 cm long. This resonant reflector was mounted directly to the laser head about 5 cm from the end of the ruby through a three-point adjustable mount. Parallelism between rod and resonator, monitored interferometrically by a He-Ne laser, was adjusted after initial laser warmup to better than $\frac{1}{4}$ fringe and held steady during operation to within $\pm\frac{1}{2}$ fringe, so long as the laser fired at regular intervals. No attempt was made to optimize the various optical spacings of the resonant reflector. A tendency of the output to jump between adjacent cavity modes from shot to shot was minimized by controlling the rod-coolant temperature. Holding the coolant to ± 1 °C, the spectrum consisted of two or three closely spaced axial modes, each less than 0.01 cm^{-1} wide, contained within an envelope less than 0.05 cm^{-1} wide. Under the usual operating conditions, the laser was fired once per second, delivering a single pulse of 90 nsec FWHM, 5-MW peak power, 12-mm^2 initial area, and 0.6-mrad full cone-angle beam divergence. At this repetition rate the laser rod after run-in returned to within approximately 10 °C of the coolant temperature between succeeding shots. In order to minimize multiple time spiking, an MgO-smoked glass cylinder was inserted into the flash lamp cavity. This diffuse pumping of the ruby, at an expense of a factor of about 1.6 in pump power compared to the original focused (via a polished elliptical cylinder) pumping, resulted in a single, essentially triangular output pulse and in addition improved its spatial uniformity and collimation. The Raytheon power supply was voltage regulated to $\pm 0.1\%$. At an operating pump power of 8% above threshold, the laser pulse height reproduced to $\pm 10\%$ at a rep rate of one per five secs and to $\pm 30\%$ at one per sec. The flashtube life ranged from 20 to 400 K shots at initial loadings of 1.6 kJ (1 MF charged to 1800 V in pulses lasting approximately 1 msec. Cold tapwater was used to cool the ruby to approximately 10 °C while a heat exchanger (demineralized, distilled water-to-cold tap water) cooled the flashtube. Use of distilled rather than tap water as flashlamp coolant appreciably extended the flashlamp life.

Unsupported split mica was used to provide the desired laser beam polarization, both $\frac{1}{4}$-wave and $\frac{1}{2}$-wave plates being used. The beam itself was found to be better than 95% plane polarized when fused quartz resonant reflector flats were used. Substitution of available sapphire flats, which however were not Czochralski grown, reduced the pump requirements somewhat, but their poor internal optical quality resulted in an output beam only 70% polarized.

A polished Corning 2-64 filter (red transmitting) reflected (at 45 °, p polarization) a small fraction of the beam into a monitor channel. The main portion of this reflection was detected by an RCA 925 vacuum phototube operated with $B+=900$ V. The resulting electrical signal, initially in excess of 20-V peak, was shaped to have a rise time of 0.1 μsec, a flat 1 μsec, 3 V top, and a decay time of 3 μsec. It served both as the "B-time-base" trigger for a Tektronix 555 dual-beam oscilloscope and as the coincidence gate for the analog-to-digital converters (ADC's). The scope was operated with its "A time base" triggered by noise picked up when the flashlamp was triggered, and its "B time base" in the "delayed triggerable" mode. A small fraction of the monitor beam was reflected (at 45 °, s polarization) from a glass cover slip and passed through a 4-mm-thick crystal of ADP oriented to produce phase-matched second-harmonic generation. The blue light thus produced was detected by a 1P28 phototube whose output was fed to one of the ADC's. This provided a monitor of the second-harmonic efficacy of each laser pulse, both as regards its amplitude and to some extent its coherence properties.

The main laser beam was deflected upward by a TIR prism and brought to focus with a 15-cm focal-length simple lens in a transparent liquid sample situated in front of the monochromator entrance slit. The beam was absorbed in $CuSO_4$ just above the sample. The glass cell containing the sample was immersed in a large, liquid-filled flat-sided glass vessel which served as a thermal bath and also minimized reflection losses. A front-surface spherical mirror positioned within the outer vessel imaged the laser "focal cylinder" onto the monochromator entrance slit. When conducting experiments in which the temperature was varied, a lens positioned just outside the larger cell replaced the front surface mirror. A field lens was used at the monochromator entrance slit. A collection solid angle of $\frac{1}{3}f$, determined within the sample, was possible. At 4× magnification, both the monochromator aperture ($\frac{1}{10}f$) and entrance slit (≤ 0.2mm) were fully illuminated. The scattering angle in all cases was 90 ° (± 12 ° due to the combined laser and scattered-beam

divergences). The monochromator, a Spex model 1700, had a 75-cm focal length, was equipped with a Jarrell Ash 13-231 grating (7620 l/in., 80× 190 mm ruled area, 59° blaze), operated in 16th order, and had a spectral dispersion of 1.3 Å/mm (11 cm^{-1}/mm at 3471 Å). To achieve theoretical resolution even at slit widths of 50 μ (~10 times the diffraction-limited width) half the grating had to be masked (reducing the quoted solid angles). This was due largely to a nonflat grating, but in part to the aberrations of the Czerny-Turner optical system, both effects being exaggerated by the short focal length and large grating angle. A straight entrance slit was used because the image of the laser focal cylinder was itself a long straight line having no excess width. In order to utilize the available slit height without sacrifice of resolution it was then necessary to curve the exit slit. The jaws for this slit were constructed of brass shim stock cut to the proper radius by a razor blade attached to a pivot arm. They were affixed with double-sided Scotch tape to the slightly opened original-equipment straight-jawed exit slit. Examination with a microscope revealed that these rather simple jaws were parallel to ±2 μ and had edges smooth to ±2 μ. They served admirably for widths down to the minimum required by the experiment, 50 μ. Also because of the large grating angle and short focal length, the entrance and exit slits when in proper adjustment were not of equal width, the ratio of their widths being $\cos(\theta-\varphi)/\cos(\theta+\varphi) \cong 1/1.7$. Here, θ is the angle between the grating normal and the instrument optic axis (~60°) and φ is $\tan^{-1}D/2F$ (~5.7°), D being the distance between the slits and F the instrument focal length. Overlapping orders higher than the 17th were heavily attenuated by the $CuSO_4$ filter used to eliminate scattered and stray laser light, while the 13th and lower orders were attenuated by a Corning 7-54 filter and the $CuSO_4$. The 14th, 15th, and 17th orders were not discriminated against but periodic checks were made assuring their absence. These were done using various Corning filters and plexiglass to alternately attenuate the various orders. The instrument transmission efficiency, including all filters, was ~20% for radiation polarized parallel to the rulings and ~12% (ratio 1.74) for the perpendicular polarization. A 2× 2× 2-cm calcite Rochon prism and a lens spatially separated the two polarization components of the monochromator output. They were measured by independent RCA 8575 photomultipliers. The phototubes were selected for their high quantum efficiency (~30%) in the blue. Operated cathode grounded, at room temperature, and with an electron gain of 4×10^7 ($B+\approx 2800$ V), they had a dark-current count rate after pulse-height discrimination at approximately 80% counting efficiency of only 10^2–10^3 per sec.

The three phototube outputs (one for each polarization of the EHLS and one for the SHG monitor) were coupled through long cables and an R-C shaping network to the ADC's (Technical Measurements Corporation, Model 210). The ADC output consisted of 4-MHz clock pulses, whose number was linearly proportional to the integral (over the duration of the coincidence pulse) of the input. The clock pulses were accumulated in electronic counters (Hewlett Packard Model 5203L), giving a visual digital readout of the signals for each laser firing. The counters could be made to reset after each shot or to accumulate over a preset number of successive shots. Under standard operating conditions, a single photoelectron from the 8575 photomultiplier produced an average signal of 30 on the counters for the signal channels while the monitor signal was adjusted to register a count of ~300 (corresponding to many thousands of photons). Although operating in a gated or coincidence mode, the ADC's converted twice on each flashlamp firing. The first conversion occurred as a result of noise picked up when the flashlamp was triggered. The counters, however, were gated by the oscilloscope B-time base and hence failed to register this noise signal. However, the pickup was large enough to cause an overdrive which had not quite relaxed by the time the desired signal and coincidence gate pulse arrived. Thus with no input, the scalers registered approximately 25 counts on each laser firing. This constant background was subtracted automatically from each reading by adjusting the ADC "baseline" control. Other useful features of the ADC's included a built-in step attenuator for calibrated gain control, a threshold control which permitted rejection of phototube noise pulses whose amplitude was small compared to that of an "average" photoelectron, and an adjustable "upper-level" limit which when exceeded cancelled the conversion. Thus, full pulse-height discrimination was available and the apparatus could be used for conventional "photon counting." For this purpose, the scaler was connected to the ADC "address reset" output which provided a single pulse whenever conversion of a photoelectron occurred. Also, by connecting all three upper-level circuits in parallel, an excessively large signal (as would result when a spark occurred in the sample) on any channel would inhibit the conversion on all three channels. The units did, however, require longer coincidence pulses than would normally have been used. Thus, although the laser pulse lasted only 0.1 μsec, the ADC's sampled the phototube output, including dark current, for ~2 μsec. Even so, phototube dark current amounted to only one spurious event per thousand laser flashes and was negligible as a noise source. For proper operation of the ADC's, the coincidence pulse had to precede the signal pulse. This feat was accomplished by overdriving the 925 phototube that produced the coincidence pulse and by keeping

its cables short while delaying the output from the signal detectors through use of long cables. The *R-C* circuit needed to shape the phototube output to meet the ADC input requirements also helped delay the signal. Power for the ADC units, which are actually plug-in modules for TMC's larger pulse-height analyzers and consequently are not self-powered, was obtained from a bank of Harrison Laboratories's adjustable regulated power supplies.

B. Procedure

The samples were prepared by distilling reagent materials (spectro- or chromato-quality when available) and filtering the distillates through 0.22-μ GSWP or 1.5-μ OHWP Millipore filters directly into all glass cells. The laser intensity was adjusted, using Corning glass filters, to the point at which dielectric breakdown within the sample occurred very infrequently. For many materials, the refuse produced by a single such breakdown would reduce the dielectric strength of the sample enough to necessitate its change. Typically the laser had to be attenuated to less than 1 MW ($\leq 1.5\times10^{10}$ W/cm^2 at focus) to prevent breakdown. Elevated sample temperatures were obtained by using an immersion heater placed inside the larger glass cell, which, except for the optical ports, was encased in $1\frac{1}{2}$ ins. of Styrofoam. The temperature was then controlled to ± 1 °C.

To obtain the spectral profile of the EHLS, the laser was fired repeatedly with the monochromator at a fixed wavelength setting until the totalized signal on the monitor channel reached some predetermined level. The accumulated signals were transcribed, the counters reset, the wavelengths advanced, and the procedure repeated. In an effort to average long-term equipment drifts, several scans through the line were made, each in the direction of increasing wavelength. Depending on the strength of the signals obtained, as many as 200 laser firings might be taken at each wavelength setting. For each wavelength, the accumulated signals for the many scans were totalized, normalized first for the number of stops at that wavelength and then normalized to one at the peak of the line.

The noise in the data was entirely statistical since even for the strongest scatterers, the peak accumulated signal corresponded to no more than a few hundred photons. Thus only the simplest of line-shape analyses was warranted. On the basis of the preceding theory, the true line shape near center was expected to be Lorentzian. Therefore, the instrumental band-pass function, measured to be triangular to very good precision over the range of slit widths used, was convoluted via computer with a family of Lorentzians of varying half-widths, generating a family of "expected" line profiles. The member which best fit the data was then selected visually, allowance being made for a possible wavelength-independent background. The width of the Lorentzian selected on this basis was then used to compute a relaxation time according to $\tau_R = 100/3\pi\Delta\nu_{1/2}$ psec, where $\Delta\nu_{1/2}$ is the Lorentzian FWHM in cm^{-1}.

C. Results

Typical data are shown in Fig. 2. Here the sample is room-temperature water, the laser was fired approximately 150 times at each wavelength setting, and approximately 300 photoevents were accumulated at the line center. Probable errors, based solely upon the statistical fluctuations to be expected in the accumulated number of photoevents, are shown for selected data points. Adjacent data points have not been averaged together and hence are statistically independent. Note the extremely high datum just left of the line center. In fitting the shown curve to the rest of the data, this point was assumed to be a statistical deviate (its deviation is <3.5 times the probable error, which has a probability of occurrence of $\frac{1}{53}$, whereas 21 data are shown) and ignored. This was done, however, only after obtaining another spectrum (using even narrower slits so that on the average the trace was even noisier) demonstrating the same sample-contributed width. The extreme-right data point demonstrates that for this example there is no need to consider a wavelength-independent background. Further out in the wings, the signal fell to less than one photoevent per 100 laser firings. This is comprised of system noise (due in part to phototube dark current, in part to stray light) and inelastic HLS.

As mentioned, at these signal levels shot noise was the dominant noise source. At higher signal levels, however, a systematic error was encountered which in fact implied a slightly less-than-linear relationship between the EHLS signal and the monitor. Two factors contribute to this. First, the monitor channel records phase-matched coherent SHG rather than EHLS. Hence, it depends differently upon the coherence properties of the laser than does the signal. Further, stimulated Brillouin scattering[29] was occurring in the sample on each laser shot. Depending upon the degree of saturation of the effect, as the laser intensity increases it prevents proportionately more of the laser beam from reaching the focal region. This systematic error became unimportant to the actual experiment when the laser intensity was controlled to $\pm 50\%$.

Except for carbon tetrachloride, it proved impossible to obtain useful data when operating the laser at levels below the threshold for stimulated Brillouin scattering. In that instance, however, the measured relaxation time and polarization

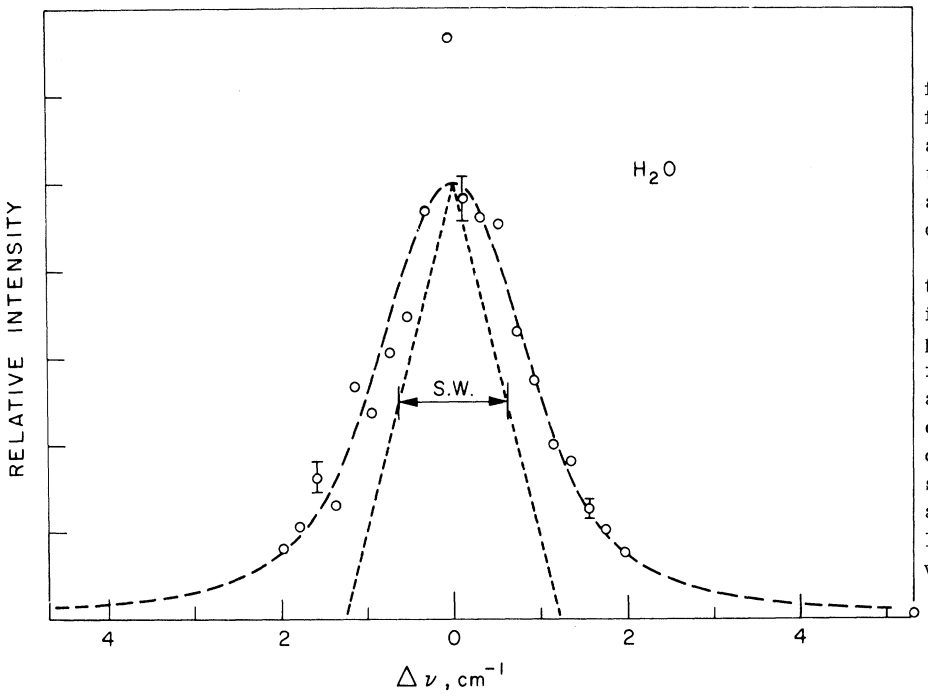

FIG. 2. Spectrum of EHLS from water. Here and in later figures the scattered radiation and laser were plane polarized in the same direction; the scattering angle was 90°; the abscissa is the displacement from 28 800 cm^{-1} (twice the laser frequency); and the ordinate is the relative EHLS intensity. The circles are unprocessed data and the error bars represent statistical uncertainties arising from the finite number of events recorded. The long-dashed curve is a convolution of the instrument bandpass function [a triangle (short-dashed curve) with FWHM equal to the indicated slit width (S. W.)] with a Lorentzian.

ratio were found to be independent of the occurrence of stimulated Brillouin scattering. Possible influences of this competing effect upon the results of the measurements will be considered further in the next section. Stimulated Raman scattering was never observed, nor were effects that could be associated with self-trapping.

Table I summarizes the data.[30–38] Column 1 gives the sample, followed by its temperature. Column 3 gives the measured polarization ratio ρ [see discussion following Eq. (45)]. The uncertainty here is simply statistical. Column 4 lists the true Lorentzian FWHM inferred from the curve fitting, followed in the next column by the associated relaxation time. Here the listed errors are qualitative estimates reflecting the quantity and quality of the data and the degree to which it could be accounted for with the computed family of profiles. Column 6 gives $\tau_0 \equiv l(l+1)\tau_{\text{meas}}$, where $l=1$ for $\rho=1.5$ and $l=3$ for $\rho=9$, while in Columns 7 and 8 appear literature citations for orientational relaxation times. There, τ_0 is twice τ_{DR}, the dielectric relaxation time or six times τ_{DRS}, the relaxation time measured from depolarized Rayleigh scattering.

For several reasons, no intensity measurements are reported. First, it was felt that the accuracies quoted in Ref. 1 could not be surpassed, nor in fact approached. This was due chiefly to the additional difficulties imposed by use of extremely narrow slits. Second, the aforementioned presence of stimulated Brillouin scattering greatly complicates any intensity measurements.

IV. DISCUSSION

A. Departures of the Sample from Its Equilibrium State Caused by the Presence of the Laser Beam

To some extent, the material properties being measured are themselves influenced by the presence of the intense-focused laser beam. Such effects result in data which do not characterize the equilibrium state of the sample. It is, therefore, important to have a good estimate of the various effects the laser beam can have upon the sample's physical state. There are several means by which the laser can exert such influence. Among the most important are by heating the sample via absorption of the fundamental beam, by causing changes in the molecular distribution functions via its electromagnetic fields, and by creating an intense hypersound wave via stimulated Brillouin scattering (SBS).[29] Let us examine each effect.

All of the liquids dealt with had good transparency at the laser wavelength. As a worst case, if 1% of the laser beam were absorbed per cm and if there is no thermal conduction or convection, then at the focus of the laser the sample would experience a temperature rise of 5 °C. For a more typical case, the rise would be less than 1 deg. In itself, such a temperature change has negligible effect on the measurements. Also, since the appropriate relaxation times in the materials studied are of the order of 10^{-11} sec, the rate of temperature rise (which may be as high as 10^8 deg/sec)

probably is not significant and the system may be regarded as being in equilibrium at all times with respect to this source of heat input. However, the sample cannot flow quite rapidly enough to accommodate the associated thermal expansion; there results a localized pressure buildup. Assuming no flow whatsoever and a 1 °C temperature rise, the pressure would reach ~ 10 atm. Such a pressure disturbance will propagate outward at sonic velocities, typically 10^5 cm/sec, so that during the laser flash it will have traveled ~ 10^{-2} cm, or a distance roughly equal to the laser focal diam. The expected pressure rise might thus be of the order of a few atmospheres. To have noticeable effect on the properties being measured, however (except when dealing with a critical point), pressures on the scale of hundreds to thousands of atmospheres are necessary.[39] Thus, absorption of the laser beam should have no significant effect on the results.

Consider next the importance of the laser beam's electric field. At focus it reaches 10^4 esu. Its most apparent influence is the alignment of molecules due to any anisotropy in the polarizability.[40,41] The interaction energy producing such alignment is given by $\alpha(\vec{\Omega})E^2_{\text{loc}}$, where $\alpha(\vec{\Omega})$ is the orientation-dependent molecular polarizability and $\vec{\Omega}$ the orientation relative to $\vec{E}$. For typical cases, this energy will vary with orientation by less than 1 % of kT_{room}. Of comparable importance is the effect of the fields on the pair correlation function.[42] Perhaps the largest term entering here is that due to the dipole moment induced by the field on one molecule interacting with the permanent (or induced) dipole moment of a neighbor. This energy, $(\alpha E\mu / r^3)$, again is of the order of 1 % of kT_{room}. It is difficult to appraise the true significance of even such small perturbations as these on the microscopic behavior of a liquid. This would again be particularly true in the vicinity of a phase transition. Hopefully, they too will have negligible effect on the measurements.

Lastly, the laser is observed to cause SBS[29] at each firing. In this process, a photon from the laser beam is absorbed while a hypersonic phonon (propagating parallel to the laser beam) and a new photon (propagating antiparallel) are created. Both momentum and energy are conserved so that, knowing the phonon velocity, its energy can readily be calculated. The rate at which this process proceeds depends upon the laser intensity. At very high intensities, much of the beam is converted, and in fact it can become completely depleted before reaching the focus. Thus, due to SBS, the laser intensity at the focal volume is reduced while at the same time the volume of sample being observed via EHLS is subjected to an intense hypersonic wave. As no intensity measurements are reported, the attenuation of the laser beam may be ignored. To obtain a worst-case estimate of the effects of the sound wave, assume that the laser beam is completely depleted, that the photon lifetime is infinite, and that the sample is subjected to the full intensity of the resultant sonic wave. Then for a typical substance, the acoustic intensity will be ~ 200 kW/cm^2, producing particle excursions of ~ ± 6 Å, acoustic pressures of ~ ± 500 atm, and modulations of the average interparticle distance of ~ ± 3 %.[43] The periodic motion of the molecules phase modulates the induced nonlinear polarization giving rise to sidebands in the scattering, separated from twice the laser frequency by the sound-wave frequency. Since the excursion is always a small fraction of the optical wavelength, the sideband intensity will be very small – of the order of parts per ten thousand – and hence can safely be disregarded. Of far greater importance seems the effect the periodic pressure-density modulation might have upon the molecular distribution functions. Note, however, that thermal agitation within a molecular volume produces pressure fluctuations of the order of thousands of atmospheres. Thus, this maximum acoustic overpressure, though a severe perturbation, would probably have no really drastic consequence. This is the worst possible case. In practice, only 10–20% of the laser beam is converted and while no quantitative account has been given, it is felt that the actual acoustic intensity present in the focal volume simultaneously with the laser is only a small fraction (~1%) of the maximum value. Further, considering that the lifetime of the created phonons is but ~ 10^{-9} sec, the maximum intensity is further reduced, and by a large factor. If the entire phonon wave were dissipated as heat in the focal volume, its temperature would rise a mere 0.01 °C. The worst case, then, is really a gross overestimate and one may confidently expect that SBS will not seriously influence the results. In fact, for one sample, this hypothesis was tested and found to hold. The EHLS signal from CCl_4 was strong enough that useful data could be obtained both above and below its relatively high SBS threshold. Within the experimental accuracy, no differences in polarization ratio or linewidth were found.

Two other mechanisms through which the laser might influence the physical state of the sample are stimulated Raman scattering (SRS)[44] and optical self-trapping.[45] No SRS was observed to occur during any of the measurements. Its absence has been taken by other workers[46] to imply that optical self-trapping does not occur.

If, for any reason, the results reflect laser induced nonequilibrium sample conditions, they will be sensitive to the average laser intensity over and above the simple square-law intensity dependence expected. Except in the above-mentioned instance, the EHLS signals were simply too weak to permit experimental investigation of the situation. In each of the several instances in which the depen-

dence of the integrated EHLS signal upon laser intensity was measured, the expected quadratic behavior was found, within the rather large shot-noise-governed experimental uncertainty.

In view of the foregoing discussion, the experimental results will most probably reflect properties of the equilibrium state of the samples measured. However, the close proximity of disaster demands that the situation in this regard be carefully reexamined for each particular sample. Small excess optical absorption or a nearby phase transition could easily swing the balance to just the opposite conclusion.

B. Relation between Various Relaxation Times

In Sec. II it was shown how the normalized $l=1$ and $l=3$ EHLS spectra relate in general to the Fourier transforms of the $l=1$ and $l=3$ spherical components of $G(\vec{\Omega},t)$, the spatially averaged orientation-dependent pair correlation function. Because of the limited amount and precision of the data, it was possible to determine only some average width for the spectra. The much simplified theory that assumes vanishing orientational correlations and isotropic orientational diffusion predicts pure-Lorentzian line shapes deriving from exponentially decaying correlation functions. On that model, the relaxation times for the degree l spherical components of $G(\Omega,t)$ are related by $\tau_l=\tau_0/l(l+1)$, $l\neq 0$, so that $\tau_1:\tau_3=12:2$.

In a manner exactly parallel to that given in Sec. II, it can be shown that the normalized depolarized Rayleigh spectrum gives $g_2(\Delta\omega)$, the Fourier transform of $\vec{G}^{[2]}(t)$.[11-15] Thus, the time behavior of the first three spherical components of $G(\vec{\Omega},t)$ are in principle available. In the approximation described above, the decay time inferred from a Lorentzian fit of the depolarized Rayleigh scattering spectrum should fit the relation $\tau_1:\tau_2:\tau_3=12:4:2$.

The dielectric decay time τ_{DR} as measured via the frequency dependence of the dielectric loss factor, is closely related to τ_1, but differs from it for two significant reasons. As detailed in the papers by Glarum[47] and Cole,[21]

$$\tau_{DR}=[(\epsilon_0+2)/(n^2+2)]\tau_\Phi, \tag{46}$$

where ϵ_0 is the dc dielectric constant, n the refractive index, and τ_Φ is the decay time for

$$\Phi(t)\equiv\langle\vec{\mu}(0)\cdot\vec{M}(t)\rangle/\langle\mu(0)\cdot\vec{M}(0)\rangle\ , \tag{47}$$

assuming that $\Phi(t)$ is an exponentially decaying function. $\Phi(t)$ is the correlation function of a permanent molecular dipole moment $\vec{\mu}$ and the total dipole moment $\vec{M}$ of the specimen. However, $\vec{M}\equiv\vec{m}+\vec{X}$ consists of two parts. $\vec{X}$ results from long-range dipole forces extending throughout the medium while $\vec{m}$, the remainder and source for $\vec{X}$, is localized about the test molecule. If the sample is large compared to the focal volume, correlations produced by $\vec{X}$ will not influence EHLS. Thus, τ_1 as measured by EHLS relates to the localized dipolar correlations only. $\vec{G}^{[1]}(t)$, as employed throughout this paper, is to be given similar interpretation. Further, $\vec{x}_d$ – that part of $\vec{X}$ due to orientation of molecules – has a delayed response to changes in $\vec{m}$ and hence causes $\vec{m}$ and $\vec{M}$ to have different time behavior. A second disparity between τ_{DR} and τ_1 results from the fact that $\vec{m}$ includes an induced polarization term, i.e.,

$$\vec{m}=\sum_{\text{loc}\,i}(\vec{\mu}+\vec{\alpha}\cdot\vec{R})_i\ , \tag{48}$$

the sum over nearby molecules of their *total* dipole moment. Here $\vec{R}$ is the reaction field produced at the molecular origin by the surrounding dielectric in response to $\vec{\mu}$. Again, part of $\vec{R}$ has delayed response to changes in $\vec{\mu}$. Using the methods of Cole and Glarum, both effects can be accounted for, and it can be shown that

$$\tau_\Phi=\frac{\epsilon_0}{\epsilon_\infty}\frac{2\epsilon_\infty+1}{2\epsilon_0+1}\frac{\epsilon_\infty+2}{\epsilon_0+2}\tau_{\varphi'}\ , \tag{49}$$

where

$$\varphi'(t)\equiv\langle\vec{\mu}(0)\cdot[\vec{M}(t)-\vec{X}_d(t)]\rangle/\langle\vec{\mu}(0)\cdot[\vec{M}(0)-\vec{X}_d(0)]\rangle \tag{50}$$

and $\varphi'(t)$ is assumed to behave like $e^{-t/\tau_{\varphi'}}$; and

$$\tau_{\varphi'}=\frac{2\epsilon_0+1}{2\epsilon_\infty+1}\frac{3\epsilon_\infty}{2\epsilon_0+\epsilon_\infty}\tau_1\ , \tag{51}$$

where $\vec{G}^{[1]}(t)$ is assumed to be given by e^{-t/τ_1} and is identified with $\langle\vec{\mu}(0)\cdot\vec{m}'(t)\rangle/\langle\vec{\mu}(0)\cdot\vec{m}'(0)\rangle$, $\vec{m}'$ being $\sum_{\text{loc}\,i}\vec{\mu}_i$, the sum over a localized region of all permanent dipole moments. Combining these relations,

$$\tau_{DR}=[3\epsilon_0/(2\epsilon_0+\epsilon_\infty)]\tau_1\ . \tag{52}$$

Equation (52) does not depend upon assumptions as to the nature of the correlations or the mechanism of relaxation and, provided only that the various correlation functions are adequately described by exponentials, it should be rather general. However, a major violation of (52) occurs if the mo-

lecular site symmetry does not define a directed axis. In that case $k \neq m \neq 0$, and the anisotropy permits as many as three different τ_1's. Only if the permanent dipole moment and the $l = 1$ element of β_{ijk} are parallel (or antiparallel) will Eq. (52) hold. The derivation also assumes the usual "spherical" dielectric sample. This has implications with regard to the ratio between the applied and internal electric fields and to the ratio between localized and "long-range" dipole correlations.

The orientational motions of molecules in liquids contribute also to the broadening of NMR,[13,23,24,48] IR absorption, and Raman scattering lines.[11,15] In each case, comparisons with various elements of $G_{km}^{[l]}(t)$ are possible, but are not always straightforward. In the IR and Raman spectra, excited vibrational states are involved. This has several important consequences.[15] First, because of the phase uncertainty so introduced, the effects are totally incoherent and only $G_S(\vec{r}, \vec{\Omega}, t)$ can contribute to the line broadening. Second, the particular spherical element of $G_S(\vec{r}, \vec{\Omega}, t)$ being measured is determined by the symmetry species of the vibrational states involved. Finally, the local environment can affect the energy levels (in a number of ways) and thus contribute a line broadening in addition to that produced by orientational motions alone. In the case of NMR relaxation, the nuclear spin system couples to the molecular motions through the quadrupole coupling coefficient, a second-rank spherical property tensor. Thus, $G_{km}^{[2]}(t)$ is involved, but, again, alternative line-broadening mechanisms exist. Further, the measured relaxation time is related to the appropriate molecular relaxation time by an extremely small coefficient, whose value depends upon both the NMR relaxation theory and upon additional experimental data.

The Brownian diffusion mechanism of orientational relaxation is found to be inappropriate in many instances, and alternative models have been proposed. Notable among these are various "jump" models, for which solutions for $G_S(t)$ usually can be given, using methods like that leading to the development of Eq. (28). However the very fact that Brownian diffusion is an inadequate approximation implies strongly that in these instances short-range orientational correlations exist and hence that $G_d(\Omega, t)$ will play an important part in the EHLS. In view of the qualitative nature of our data and in the absence of good models for $G_d(\Omega, t)$, there seems little point in attempting to identify mechanisms other than pure Brownian diffusion.

C. Higher-Order Nonlinearities

In all of the foregoing, it has been assumed that the sole source for the component of dipole moment at 2ω is the term $\beta_{ijk} E_j(\omega) E_k(\omega)$. Several authors[5,7] have in addition considered terms like $\gamma_{ijkl} E_j(\omega) E_k(\omega) F_l(t)$, where $\vec{F}(t)$ is the time-dependent instantaneous local electric field which exists in the absence of any external fields. When the molecules possess permanent dipole moments, $\vec{F}$ includes the reaction field $\vec{R}$ mentioned above. Just as the dipole moment was enhanced by $\vec{\alpha} \cdot \vec{R}$ in the calculation of dielectric relaxation, so $\vec{\beta}$ will be enhanced by $\vec{\gamma} \cdot \vec{R}$ in a calculation of EHLS. Similarly, since $\vec{R}$ has delayed response to motions of the test-site molecule, not only will the intensity of the EHLS be enhanced, its spectral width will be narrowed (or broadened, depending upon the sign of the relevant tensor elements). Representing the measured relaxation time by τ_m and the corresponding orientational relaxation time by τ, then, from the response function theory of Cole,[21]

$$\Delta\tau_m/\tau = (\tau_m - \tau/\tau) = \Delta\beta/\beta = \gamma R/\beta \ . \tag{53}$$

Since, $\Delta\tau_{\varphi'}/\tau_1 = \Delta\mu/\mu = \alpha R/\mu$,

$$\Delta\tau_m/\tau = (\gamma\mu/\alpha\beta)\Delta\tau_{\varphi'}/\tau_1 \ , \tag{54}$$

and in addition $\gamma\mu \cong \alpha\beta$, we see that

$$\Delta\tau_m/\tau \cong \Delta\tau_{\varphi'}/\tau_1 \ . \tag{55}$$

While this correction term of course depends upon the tensor nature of α, β, and γ, the corrections involved will be of the magnitude $\tau_{\varphi'}/\tau_1$.

The reaction field just discussed was correlated to the motion of the test-site molecule and hence, merely altered an existing term. $\vec{F}$ includes uncorrelated, random terms as well. They will contribute to the scattered intensity a term proportional to $\{\gamma(0) \cdot \vec{F}(0)\} \times \{\gamma(t) \cdot \vec{F}(t)\}$. Since the time scale for fluctuations in $\vec{F}(t)$ corresponds to that for molecular collisions, this term will produce a very broad (~ 100 cm^{-1}) spectral component, which feature might serve to identify it.

It is of interest to note that in a monatomic fluid like liquid argon a major fraction of $\vec{F}$ will arise from pair interactions. Since a pair of identical atoms possesses inversion symmetry, that fraction of $\vec{F}$ cannot contribute to $(\gamma F)^2$ EHLS. Should EHLS be seen in such a system, it must reflect three, or more, particle interactions.

D. Individual Results

1. *Water*

The EHLS spectrum for water at 22 °C appears as Fig. 2 and has already been discussed. As seen in the figure, a relatively good fit of the data to the convolution of a Lorentzian with the instru-

ment's response function was obtained. The derived relaxation time and the measured polarization ratio are given in Table I, together with the results of measurements made with the sample at 60 °C.

From the polarization ratio, $\rho = 8.6 \pm 0.6$, it is apparent that the present experiments measure τ_1, the relaxation time of the dipolar-correlated molecular subset. As discussed on rather general grounds in the preceding paragraphs, τ_1 and the dielectric relaxation time τ_{DR} are related by $\tau_1 = (2\epsilon_0 + n^2/3\epsilon_0)\tau_{DR}$. Using the well-established value of τ_{DR},[30] this predicts that at 22 °C $\tau_1 = 5.9$ psec. The measured value, 8.8 ± 0.8 psec is roughly 4σ larger. The disagreement, while not quite so large, persists at 60 °C, so that little doubt remains as to its reality. Since the water molecule possesses a directed symmetry axis (as do current models of the local structure of liquid water), it cannot be argued that this difference is due to the fact that $\vec{\vec{\mu}}$ and $\vec{\vec{\beta}}^{(1)}$ are not parallel. There remains the influence of higher-order terms. If the reaction field $\vec{R}$ were of the same importance in determining $\vec{\beta}_{\text{tot}}$ as it is in determining $\vec{\mu}_{\text{tot}}$, the predicted relaxation time for 22 °C water would be 6.9 psec, still 2.5σ too small. Assuming that $\vec{\vec{\beta}}^{[1]}$ and $\vec{\vec{\mu}}$ are parallel and that just the isotropic parts of $\vec{\vec{\alpha}}$ and $\vec{\vec{\gamma}}$ (denoted $\bar{\alpha}$ and $\bar{\gamma}$, respectively) are important, the full discrepancy can be explained if $\vec{\vec{\beta}}^{[1]}/\bar{\gamma} \cong 0.3\,\vec{\vec{\mu}}/\bar{\alpha}$. Since $\bar{\alpha}$ and $\bar{\gamma}$ are isotropic material parameters (they are finite for perfect spheres), while $\vec{\vec{\mu}}$ and $\vec{\vec{\beta}}^{[1]}$ depend upon a lack of inversion symmetry (hence they are in some measure determined by the molecular anisotropy) this would imply simply that the nonlinear electrical properties are less anisotropic than the linear. The 60 °C result is adequately fitted by this same assumption. While the above provides a reasonable account of the data, the possibility remains that the assumption implicit in Eq. (51) provides an inadequate description of a liquid as structured as water.

NMR relaxation data are available for liquid water,[23,48] the results indicating that τ_2 is about $\frac{1}{4}\,\tau_{DR}$. If one assumes the simple orientational-diffusion relation $\tau_l = \tau_0/[l(l+1)]$ and in addition $\tau_1 = [(2\epsilon_0 + n^2)/3\epsilon_0]\,\tau_{DR}$, then $\tau_2 = [(2\epsilon_0 + n^2)/9\epsilon_0]\,\tau_{DR}$ or, for water at 22 ° C, $\tau_2 = 0.22\,\tau_{DR}$. Because of the rather uncertain relation between τ_2 and the actual NMR measurements, this remarkable agreement cannot be taken as proof of the validity of the assumptions. In view of the current picture of the structure of liquid water, it is highly unlikely that simple diffusion is important, so that the relation $\tau_l = [\tau_0/l(l+1)]$ cannot be employed. A better first-approximation might be that microscopic relaxations are all dominated by the same structure-relaxation time or that $\tau_2 = \tau_1$. As discussed earlier, the spectral width of the depolarized Rayleigh scattering line gives a much more direct measure of τ_2. Because of the weakness of the scattering, however, this measurement has yet to be performed.

2. *N, N-Dimethylformide* (NNDMF)

As seen from Eq. (43), if $G_{00}{}^{[1]}(t)$ and $G_{km}{}^{[3]}(t)$ have different time behavior, the EHLS spectral profile will depend upon the direction of polarization of the scattered light. This is because the different polarizations contain different proportions of the $\vec{\beta}^{[1]}$ and $\vec{\beta}^{[3]}$ spectra. An example of this situation is shown in Fig. 3(a), which shows both polarizations of the EHLS from NNDMF at room temperature. It was the only liquid studied in which the effect was discernible. In most other materials, either $|\vec{\beta}^{[1]}|^2 \gg |\vec{\beta}^{[3]}|^2$ or vice versa, making it experimentally difficult to extract the weaker spectral component. In accordance with Eq. (43), the $\vec{\beta}^{[1]}$ and $\vec{\beta}^{[3]}$ spectra were determined from the data of Fig. 3(a) by forming $I_{\parallel} - \frac{3}{2}I_{\perp}$ and $I_{\perp} - \frac{1}{9}I_{\parallel}$, respectively. Correction for the finite collection solid angle was included. The resulting spectra, together with the best-fit Lorentzian convolutions, are shown in Fig. 3(b). The ratio of $|\vec{\beta}^{[3]}|^2/|\vec{\beta}^{[1]}|^2$ deduced in this curve-fitting process was 3.4:1, consistent with the value of (3.5 ± 0.3):1 obtained from the integrated-intensity polarization ratio.

From the widths of the best-fit Lorentzians, $\tau_1 = 5 \pm 1$ psec and $\tau_3 = 1.5 \pm 0.5$ psec. The dielectric relaxation time is $\tau_{DR} = 10.6$ psec,[31] implying on the basis of Eq. (51) that τ_1 should equal 7.5 psec. As discussed, a zeroth-order reaction-field correction can be made, but this results in even greater disagreement between τ_1 and its predicted value. However, the NNDMF molecule lacks a directed symmetry axis and it is probable that $\vec{\vec{\mu}}$ and $\vec{\vec{\beta}}^{[1]}$ are not collinear. This provides a ready explanation of the discrepancy between τ_1 and the value predicted from τ_{DR}. In fact, if the predominant force producing local structuring is the interaction between permanent dipole moments, then any component of $\vec{\vec{\beta}}^{[1]}$ perpendicular to $\vec{\vec{\mu}}$ will undoubtedly relax faster than $\vec{\vec{\mu}}$, with the resultant prediction that τ_1 should be smaller than the value predicted from τ_{DR}, which is exactly the case. In view of the low molecular symmetry, little can be said about the relative values of τ_1 and τ_3. In fact, more than one τ_3 exists – as detailed in Sec. II – the measured value being some average. Thus, little significance, one way or the other, should be attached to the fact that the experimental ratio of τ_1/τ_3, 3.3 ± 1.3, does not willingly equal 6, the value predicted by isotropic orientational relaxation.

3. *Carbon Tetrachloride*

A molecule with tetrahedral symmetry has no dipole moment nor isotropic polarizability ten-

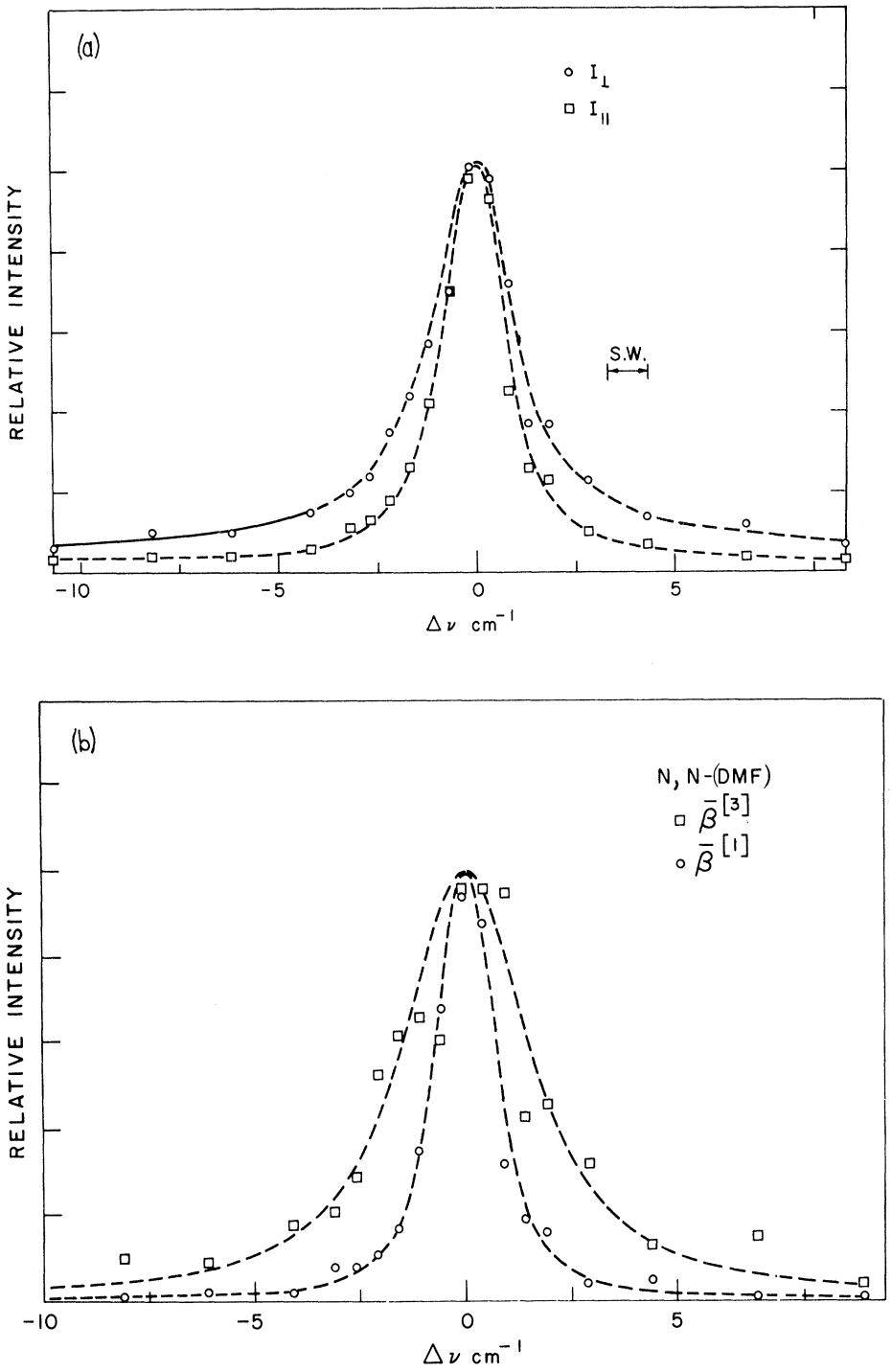

FIG. 3. EHLS spectra from *N*, *N*-dimethylformamide. (a) Scattered intensity polarized parallel and perpendicular to the direction of polarization of the laser, the points being connected by a smooth line. (b) $\bar{\beta}^{[1]}$ and $\bar{\beta}^{[3]}$ spectra derived from (a), together with the best-fit Lorentzian convolution.

sor. Thus, pure rotational motions of individual molecules do not give rise to either infrared absorption (dielectric relaxation in liquids) or to Raman scattering (depolarized Rayleigh-wing scattering in liquids). However, $\bar{\beta}_{xyz}$ does not vanish (in spherical representation $\bar{\beta}_2^{[3]} = \bar{\beta}_{-2}^{[3]} \neq 0$), and EHLS provides for the first time a means of optically studying the rotational motions of molecules like CH_4 and CCl_4. Indeed, evidence for pure rotation HLS from gaseous CH_4 has been presented,[49] and unresolved EHLS from liquid CCl_4 has been reported, by several workers.[1,7] However, the polarization ratio for the EHLS from liquid CCl_4 was found to be 2.9 ± 0.3,[1] not $\frac{3}{2}$ as re-

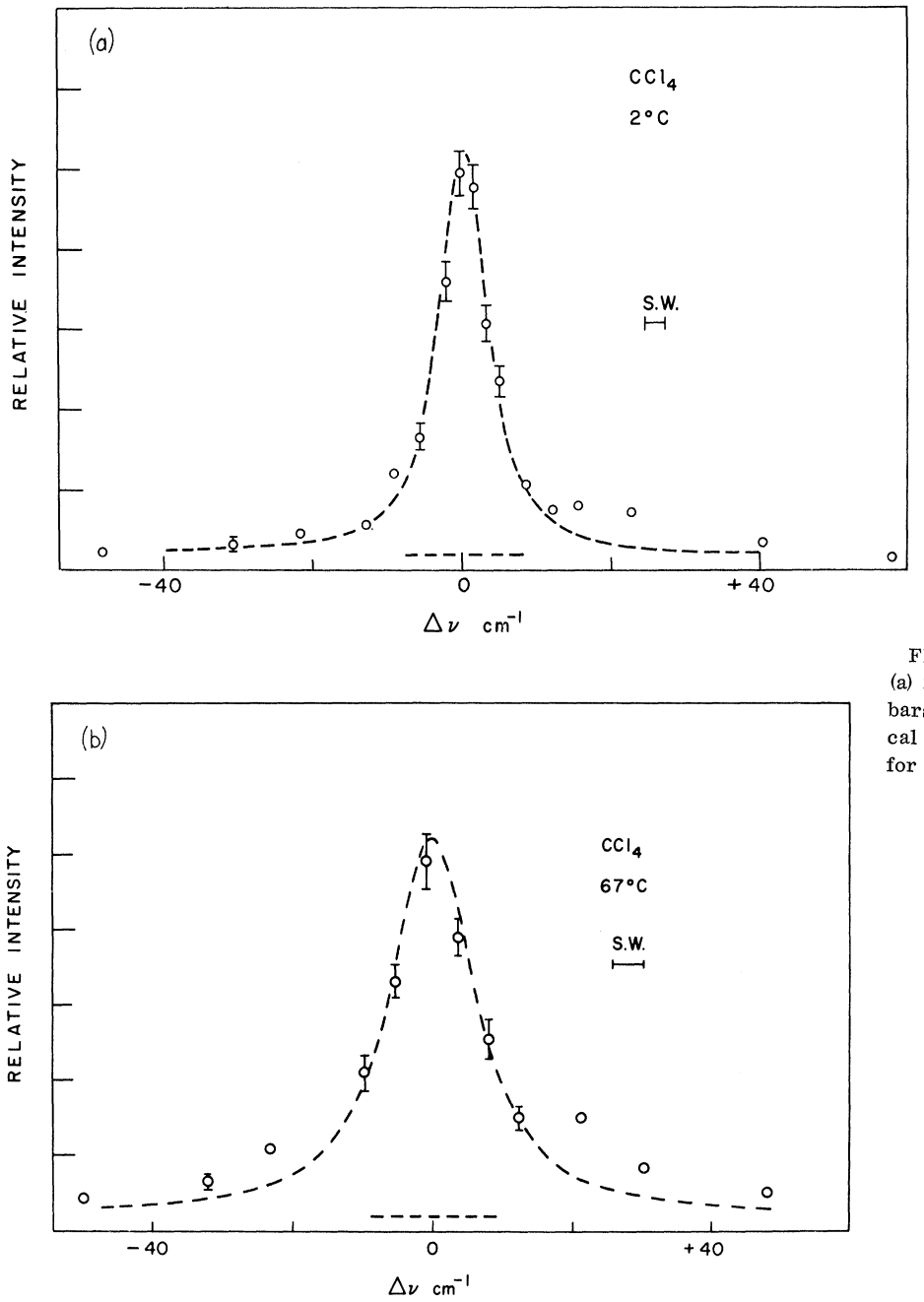

FIG. 4. EHLS from CCl_4 at (a) 2° C and (b) 67° C. Error bars representing the statistical uncertainties are shown for typical data points.

quired for tetrahedral scatters, and Weinberg[7] has shown that both the measurements on CCl_4 and CH_4 can be explained with $\bar{\beta}_{xyz} = 0$. Thus, considerable interest focuses upon EHLS from CCl_4, and a more extensive investigation was conducted for this substance.

The intensity, polarization, and linewidth were first measured as functions of sample temperature from 2 to 67 °C. The spectra obtained at the extreme temperatures are typical and are shown in Fig. 4, together with attempts to fit the data to Lorentzian line shapes as corrected for the instrumental response. The presence of a background signal is evident, and it has been included in the curve fitting. Even so, a relatively poor accounting of the line shapes results. The evident temperature dependence of the linewidth is summarized in Fig. 5, where the recorded width is that of the best-fit Lorentzian.

Background signals of nearly the magnitude found here were observed from many of the materials studied. Much larger background signals (~100

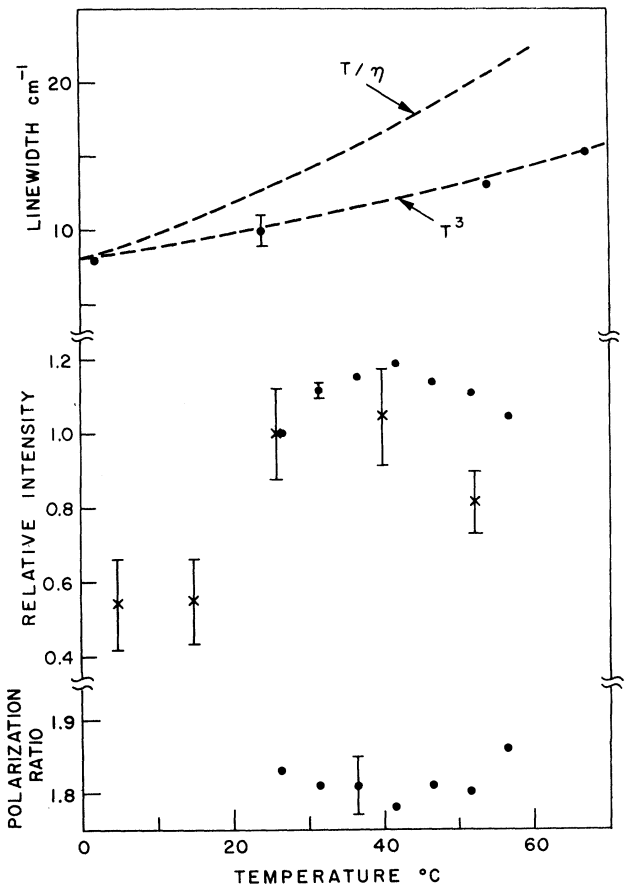

FIG. 5. Temperature dependence of the spectal half-width, intensity (o, present data; x, data of Weinberg Ref. 7), and polarization ratio of EHLS from CCl_4. Dashed lines show the temperature divided by the viscosity [A. K. Doolittle and D. B. Doolittle, J. Appl. Phys. 28, 901 (1957)] and the cube of the temperature, both normalized to the linewidth data at 2°C. Typical error bars appear.

times), probably due to nonlinearly excited luminescence, in fact totally masked the EHLS signals in benzene and its derivatives. In CCl_4, the background amounted to $\sim\frac{1}{50}$ photon per laser shot, making it difficult to study. Seemingly it extended hundreds of cm^{-1} to either side of $\Delta\nu = 0$, was largely plane polarized parallel to the laser polarization direction, was time coincident with the laser pulse, and seemed to increase slightly in magnitude with increasing sample temperature.

Some difficulties were encountered in determining the polarization ratio. These were primarily due to the fact that the background signal was polarized. Being essentially independent of wavelength, it made a greater and greater contribution to the signal as the monochromator slits were opened to provide larger signals and better statistics. Thus, the polarization ratio was a function of the resolution of the measurement. Using a spectral bandpass comparable to the true width, ρ was determined to be 1.83 ± 0.11. This value represents the average of a large body of data obtained from four totally independent experiments. In contrast, when a broad spectral bandpass ($< 100\ cm^{-1}$) was employed, the value $\rho \cong 2.9$ (that reported in the earlier paper) was approached. The narrow-bandpass polarization ratio was found to be relatively independent of temperature over the range 23–60°C, as seen in Fig. 5.

The temperature dependence of the intensity of the EHLS using a bandpass of 40 cm^{-1}, was followed between 20 and 60 °C, the results appearing in Fig. 5. A slight peaking occurred at about 40 °C, the intensity falling by about 20% at the extreme temperatures. Figure 5 also shows data obtained by Weinberg.[7] The two sets of data are similar where they overlap, but he makes the important observation that the intensity continues to fall as the sample is cooled, dropping by about a factor of 2 between 25 and 15 °C.

The spectral width, integrated intensity ($I_{||}$ only), and polarization ratio of the EHLS were determined as functions of methanol concentration in CCl_4 at room temperature. The data are shown in Fig. 6. Strikingly, the polarization ratio was observed to fall as MeOH was first added, reaching a minimum of 1.53 ± 0.05 (the tetrahedral value!) at ~10% MeOH. Also of significance, the

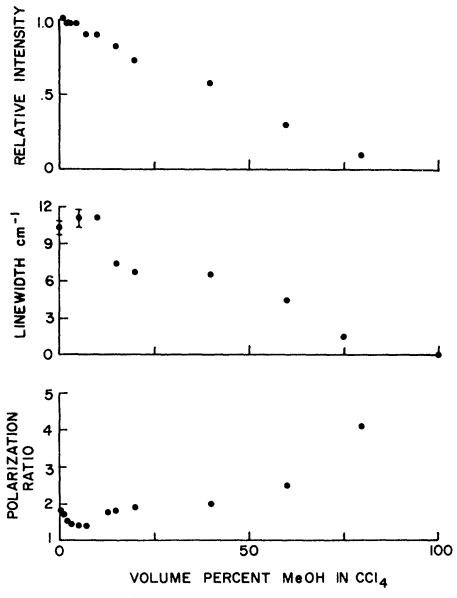

FIG. 6. Relative intensity, spectral half-width, and polarization ratio of the EHLS from mixtures of methanol in CCl_4. The abscissa gives the volume of pure methanol in the mixture, expressed as a percentage of the final volume.

integrated intensity falls essentially linearly from its highest value, at 100% CCl_4, to its lowest value, reached at 100% MeOH. The linewidth versus concentration shows perhaps an initial, gradual increase as MeOH is added to pure CCl_4, followed by a sudden drop – by almost a factor of 2 – between 10 and 20% MeOH.

To begin the discussion of these data, consider the observed background signal, common to most materials but somewhat larger in CCl_4; being highly polarized, it cannot arise from the response of individual, undistorted CCl_4 molecules and therefore must be due to interactions characteristic of the liquid state. Strauss[32] has recently observed very closely related phenomena in liquid CCl_4, namely, residual far-infrared absorption (or high-frequency dielectric relaxation) and depolarized Rayleigh-wing scattering. As mentioned, both effects vanish for perfectly tetrahedral, noninteracting molecules. The existence of residual far-infrared absorption requires that the liquid-state interactions support $l=1$ spherical tensor properties. Therefore EHLS due to such interactions will contain an $l=1$ or totally polarized ($\rho=9$) component. Presuming that all such $l=1$ effects originate from the properties of a highly transient configuration of the liquid state, they will demonstrate in first approximation identical relaxation behavior – that of the responsible configuration. Thus, the spectrum of such an EHLS component will be just the Fourier transform of the dipole-moment correlation function derived by Strauss. That function begins with a short inertial period, ends in an ill-determined tail, and in between shows a rather long period well characterized by exponential decay with a time constant of ~0.2 psec. This time is exactly the bulk- or compressional-relaxation time calculated by Nettleton.[50] Thus its Fourier transform will have roughly the appearance of a Lorentzian with FWHM of ~50 cm^{-1} ($\sim 1/\pi c\tau$). It seems highly likely that the observed EHLS background signal, being polarized and approximately this width, is in fact this component. Having made such identification, the two different polarization ratios (1.83 for narrow slits and 2.9 for wide slits) actually provide a cross check. If the background is a Lorentzian with $\rho=9$, and the main signal derives from the nonvanishing molecular constant $\vec{\beta}_{\pm 2}{}^{[3]}$ and is a $\rho=\frac{3}{2}$ Lorentzian, then to satisfy the polarization data the former must have 0.09 times the peak height and 0.45 times the integrated intensity of the latter, and must be exactly 50 cm^{-1} wide! This estimate of the width is of course subject to rather large experimental uncertainties. Further, it should not be expected to exactly equal the value derived from residual infrared absorption data, not because of the correction factors discussed earlier (which in this case are all unity since $\epsilon_0=n^2$) but because here $\vec{\beta}^{[1]}$ and $\vec{\mu}$ are not molecular constants, but derive from dynamic liquid-state interactions. There is thus no assurance that their relaxation behavior is identical. For instance, $\vec{\beta}^{[1]}$, being a nonlinearity, might well depend upon a higher power of the pair approach distance than does $\vec{\mu}$. However, it is highly probable that the EHLS background arises from exactly the same aspect of the liquid-state environment as does the residual infrared absorption.

Next, observe that the liquid-state interactions invoked above cannot arise through orientational correlations, as they were discussed in Sec. II. This is contrary to the conclusions of Bershon *et al.*,[6] but a similar result was obtained by Keliech.[5] Examination of Eq. (20), which is the general expression for the EHLS intensity in terms of the elements of the pair correlation function, reveals that regardless of the nature of the correlations, if $\vec{\beta}^{[1]}$ vanishes, then the polarization ratio must be $\frac{3}{2}$. This result follows simply from the fact that spherical harmonics do not change their degree ("l" value) under coordinate frame rotation. The same arguments apply to depolarized Rayleigh scattering and in an obvious way to dielectric relaxation – if individual molecules lack dipole moments, no group of molecules can have a dipole moment resulting from "additive" effects. Thus, a response "nonadditive" in single-molecule properties must be invoked. Several simple theoretical approaches to the handling of this problem have been introduced.[5–7,51] One such theory is embodied in the concept of a molecular field, as described in Sec. IV C. While the EHLS-background signal data represent new input to such theories, they are too limited at the present time to be of great help in their development.

Several facets of the data suggest that the "additive" coherent effects describable by the methods of Sec. II are important in the EHLS from liquid CCl_4. First, while the Debye-Stokes relation

$$\tau_l = 8\pi a^3 \eta(t)/l(l+1)kT,$$

[$\eta(t)$ being the temperature-dependent shear viscosity] is not to be taken too seriously, even for the tetrahedrally symmetric CCl_4 molecule, nonetheless the room-temperature $l=3$ relaxation time so predicted is ~30 psec,[33] one-and-one-half orders of magnitude longer than the measured value, 1.1 psec. Nor does the EHLS linewidth $\Delta\nu_{1/2} \equiv 1/\pi c\tau_3$ behave with temperature like $T/\eta(T)$, instead it raises much more slowly with T (see Fig. 5). Over the limited temperature range covered, the linewidth data could be nicely fitted by a T^3 dependence, but no importance has been attached as yet to this fact. Further, the marked temperature dependence of the EHLS intensity strongly implies local orientational ordering, as has already been noted by Weinberg.[7] The fact

that the EHLS intensity falls with decreasing temperature requires that the molecular arrangement existent at low temperatures must possess more highly developed inversion symmetry than the room-temperature configuration. Next, note in Fig. 4 that the observed line shape departs consistently and significantly in the region $|\Delta\nu| = 2\Delta\nu_{1/2}$ from the Lorentzian shape anticipated on the basis that single molecules undergoing diffusional-orientational motion produce the EHLS. Several of the other simple models of the orientational relaxation of single molecules also predict Lorentzian line shapes.[11,21,25] Thus, either a complex mode of orientational relaxation or coherent effects are implied. (In the full theory, the line shape of course is the Fourier transform of the $l=3$ spherical element of the pair correlation function, which function needn't be an exponential.) Further we observe that the correlation function for the anisotropic polarizability shown by Strauss[32] seems to have a reasonably well-defined exponential tail for $t > 0.5$ psec. The decay time of this exponential is 1.1 psec, exactly that given by the inverse of the EHLS linewidth. As mentioned earlier, the anisotropic polarizability is a property not of individual molecules but of the liquid-state interactions. While this agreement between the dominant EHLS relaxation time and a known interaction relaxation time may well be coincidental, the combined weight of the above evidence suggests that EHLS from liquid CCl_4 is strongly influenced by coherence effects, certainly so at low temperatures.

The above contention requires short-range orientational ordering in liquid CCl_4. X-ray–scattering data have long provided proof that such ordering does exist.[52-54] Two high-precision x-ray studies have recently been reported[53,54] and while the structure models they present differ, an origin for the coherent optical effects can be found in either. These x-ray studies provide a picture of only the average or static structure, but if the various optical effects could be associated with specific features of the structure, its dynamic behavior would begin to emerge. While such associations might be made using just the room-temperature data, a much more credible assignment would be possible if the temperature dependence of all the pertinent data were known and included.

Finally consider the EHLS data from CCl_4-methanol (MeOH) mixtures, as summarized in Fig. 6. While not fully understandable, it is presented as further evidence for, and against, the structured nature of liquid CCl_4 and the importance of that structure in the EHLS. MeOH was chosen as the diluent because in pure form it produced relatively weak, completely polarized ($\rho = 9$) EHLS. The fact that ρ decreases to the tetrahedral value $\frac{3}{2}$ as MeOH is first added can only mean that in low concentrations it inhibits the $l=1$ spherical tensor liquid-state properties present in pure CCl_4. Since neither the intensity nor the linewidth are changed appreciably as ρ goes to 1.5, the suspected short-range orientational correlations are either nonexistent at room temperature or are not much disturbed by the addition of 10% MeOH. When the MeOH concentration is increased from 10 to 15%, a new, local structure evidently evolves, as indicated by the rising polarization ratio and the sharply falling linewidth. Apart from the fact that it is not tetrahedral, little can be said of this structure. Throughout the entire concentration range, including this region wherein a new structure is forming, the EHLS intensity is essentially linearly proportional to the CCl_4 concentration. This carries the implication that coherent effects are of little importance at room temperature, at least not as regards the intensity of scattering.

In summary, the origin of the departure of the polarization ratio from the tetrahedral value is now understood, but the importance of coherence effects remains to be definitely established. Certain relations between the EHLS spectrum and the far-infrared absorption and anisotropic polarizability-correlation functions are noted. The possibility of understanding these relations and even the origin of the anomalous optical effects in terms of a dynamic model of the liquid structure is suggested. Determination of the temperature (and perhaps solute) dependence of the various data is of prime importance to such understanding.

4. *Further Materials*

The spectral width and polarization ratio (measured over $\Delta\nu = \pm 20$ cm^{-1}) have been measured for 10 additional liquids. These were chosen on the basis of transparency at $2\nu_I$, availability in relatively pure form, and high threshold for sparking in the as-prepared state. No benzene derivatives are included, since those tested all produced the aforementioned luminescence, which obscured the EHLS signal.

The polarization ratio for EHLS in chloroform is exactly that expected for the relaxation of an $l=3$ spherical tensor. As depolarized Rayleigh scattering[10] and dielectric loss[34] data are available, an excellent opportunity to check the applicability of a rotational diffusion model presents itself. The ratios of the $l=3$, $l=2$, and $l=1$ relaxation times [the latter corrected in accord with Eq. (51), using the value $\tau_{DR} = 5.4$ psec] are, however, 1 : 2.46 : 1.83, not 1 : 2 : 6. Thus, while the EHLS and depolarized Rayleigh linewidths are in reasonable agreement with the diffusional model, the observed dielectric relaxation time is some 3 times less than the value expected from that agreement. Further, the discrepancy cannot be explained in

terms of the tensor properties of the rotational diffusion coefficient, since, by the molecular symmetry, $\vec{\mu}$ and $\overleftrightarrow{\alpha}^{[2]}$ are both relaxed only by rotation about axes perpendicular to the figure axis and therefore should have relaxation times related by the expected factor of 3. Thus, diffusional orientation relaxation cannot account for the observed times. It might next be argued that perhaps an orientational pair correlation function exists having only a strong $l=1$ spherical component, as would result from dipolar coupling. Dielectric studies of the liquid[34] do not, however, suggest such coupling. Thus we again are led to the conclusion that either structural effects and coherent scattering exert dominant influences or that the orientational relaxation cannot be described as diffusional. The latter seems more likely.

Acetonitrile demonstrates EHLS of maximum polarization ratio ($\rho=9$), so that the relaxation of an $l=1$ quantity is being observed. Thus, the decay time determined via EHLS should coincide with the dielectric relaxation time as corrected according to Eq. (51). The corrected dielectric relaxation time is however more than 3 times shorter than the observed EHLS time. No simple explanation of this discrepancy exists; possibilities include inadequate treatment of the reaction field for this highly dipolar material and the usual structural effects. Note that the first-order effect of the pulsed laser beam upon the sample properties as discussed earlier (heating of the focal volume, intense sound waves, etc.) would probably be to shorten the relaxation time, whereas the opposite disparity is observed.

Even less can be said in the case of diethylether, where the polarization ratio indicates contributions to the EHLS from both $\overleftrightarrow{\beta}^{[1]}$ and $\overleftrightarrow{\beta}^{[3]}$. Unlike dimethylformamide, the intensity of the EHLS was too weak to permit separate determination of the two spectral profiles. The polarization ratio being nearer to 9 than to $\frac{3}{2}$ implies that the decay time deduced from the EHLS linewidth, 1.5 psec, should (assuming the diffusional-orientational relaxation) be close to, but smaller than, the corrected dielectric relaxation time. That time is in fact 1.95 psec, but such qualitative agreement is of little interpretative value in view of the complexity of the molecule.

Four other liquids produced EHLS whose spectral width could be measured (dichloromethane, methylcyclohexane 2-methylbutane, and 2-2-4-trimethylpentane). A literature search failed to produce other data on their orientational relaxation times. The relatively simple molecule dichloromethane produced pure $\overleftrightarrow{\beta}^{[1]}$ EHLS, and discussion like that given above would be possible if the other times were known. In the other instances, the molecular complexity and admixing of $\overleftrightarrow{\beta}^{[1]}$ and $\overleftrightarrow{\beta}^{[3]}$ components would rule out any significant interpretation unless the simplest relations were satisfied.

In addition, three simple alcohols (methanol, n-propanol, and isopropanol) were studied. These liquids are strongly hydrogen bonded and demonstrate dielectric relaxation times longer than 100 psec.[30,37,38] On that basis it was not anticipated that spectral broadening of their EHLS would be detected, and this was indeed found to be the case.

V. SUMMARY AND CONCLUSIONS

The spectrum of "quasielastic" second-harmonic light scattering has been shown to provide, in theory, a rich source of information about the time dependence of the orientation-dependent molecular pair distribution function of liquids. However, due to the very low intensity of the scattering, only an effective-spectra linewidth has been measured experimentally. This width translates into an average orientational relaxation time which, it is felt, represents an equilibrium property of the sample in spite of the presence of intense laser illumination. Considered together, dielectric relaxation, depolarized Rayleigh scattering, and the present measurements (however meager) provide a basis for discussing orientational ordering and relaxation in liquids, and it is found that Brownian diffusion is a poor model in almost all cases. Projected development of the experimental apparatus will permit recording the entire spectrum of the EHLS for each laser shot, and thereby increase the data acquisition rate by $1\frac{1}{2}$–2 orders of magnitude. With that improvement, it should be possible to make a quantitative study of the EHLS spectral profile and hence to determine the time dependence of both the first- and third-degree spherical elements of the pair correlation function. As the second-degree elements are available from depolarized Rayleigh scattering – a field in which experimental techniques are rapidly developing – a fairly precise picture of the first three spherical components of the dynamic orientation-dependent pair correlation function would then exist.

ACKNOWLEDGMENTS

I wish to thank R. W. Terhune, K. T. Hecht, G. W. Ford, and L. Lohr for many helpful discussions; and C. M. Savage for his invaluable aid in conducting the experiments.

APPENDIX

The transformation of $\vec{\beta}$ to spherical representation is best introduced in the expression for the energy of interaction per molecule between the nonlinear medium and the generalized triple product of the applied field amplitudes. In order to satisfy both Eq. (1) and the relation $p_i^{(\alpha)} \equiv \partial W/\partial E_{\mathrm{loc}\,\alpha i}$, the interaction energy W in Cartesian representation can be written

$$W=-\frac{1}{3}\left(\frac{n^2+2}{3}\right)^3 \sum_{i,j,k} \beta_{ijk}(E_{1i}, E_{2j}, E_{3k}) \times E_{1i}E_{2j}E_{3k}, \quad \text{(A1)}$$

where $E_{\alpha i}$, $\alpha = 1, 2, 3$, and $i = x, y, z$ represent the real ith vector component of the αth applied field (the three field amplitudes are at this point assumed to be distinguishable, as for instance by their frequencies), while the $\beta_{ijk}(E_{1i}, E_{2j}, E_{3k})$ are simply regarded as the constants of proportionality, characteristic of the nonlinear medium, between the product of field amplitude components and W. Note that due to dispersion, in general

$$\vec{\beta}(\vec{E}_1, \vec{E}_2, \vec{E}_3) \neq \vec{\beta}(\vec{E}_2, \vec{E}_1, \vec{E}_3). \quad \text{(A2)}$$

Thus, considered as a factor of (A1), the product of field amplitudes $\vec{E}_1 \times \vec{E}_2 \times \vec{E}_3$ must be considered an *ordered* product.

A unitary substitution transform is next applied to the 27-element tensorial set $E_{1i}E_{2j}E_{3k}$ so as to decompose it into irreducible (under the three-dimensional pure rotation group R_3) tensorial sets. This may be accomplished by first regrouping the Cartesian vector components of each of the field amplitudes so that they transform under R_3 like the m components of the degree one irreducible tensor. The notation of Fano and Racah[55] will be strictly adhered to, so that the *standard* vector components of $\vec{E}_\alpha$, denoted by $E_{\alpha m_\alpha}^{(l_\alpha)}$, are given by

$$E_m^{(l)} = \sum_k (lm|k) E_k, \quad \text{(A3)}$$

$$\text{where} \quad (lm|k) = \begin{pmatrix} i/\sqrt{2} & 1/\sqrt{2} & 0 \\ 0 & 0 & -i \\ -i/\sqrt{2} & 1/\sqrt{2} & 0 \end{pmatrix}, \quad \text{(A4)}$$

with $m = +1, 0, -1$, $k = x, y$, and z and $l = 1$. The irreducible products of three such standard sets, denoted by $(E^3)_m^{(l_i, l)}$, are given by[20,28,55]

$$(E^3)_m^{(li,l)} = \sum_{m_1 m_2 m_3} (l_3 m_3 l_2 m_2 | l_i m_i) \times (l_i m_i l_1 m_1 | lm) E_{1m_1}^{(l_1)} E_{2m_2}^{(l_2)} E_{3m_3}^{(l_3)}, \quad \text{(A5)}$$

where of the many vector coupling schemes available, the indicated one will be employed. Here l_1, l_2, and l_3 are of course all equal to 1 but have been left unspecified as an aid in following the development. As a remainder, the vector coupling Wigner, or Clebsch-Gordan coefficients (related to 3-j symbols) are subject to the conditions $l_i \geq 0$ and $|m_i| \leq l_i$, and satisfy the elementary relations[20,28]

$$(l_1 m_1 l_2 m_2 | l_3 m_3) = 0, \quad \text{unless } m_3 = m_1 + m_2, \quad l_3 = |l_1 - l_2| \text{ or } |l_1 - l_2| + 1 \text{ or } \cdots l_1 + l_2; \quad \text{(A6)}$$

$$(l_1 m_1 l_2 m_2 | l_3 m_3) = (-1)^{l_1 + l_2 - l_3} (l_2 m_2 l_1 m_1 | l_3 m_3); \quad \text{(A7)}$$

$$(l_1 m_1 l_2 m_2 | l_3 m_3) = (-1)^{l_1 + l_2 - l_3} (l_1 - m_1 l_2 - m_2 | l_3 - m_3); \quad \text{(A8)}$$

$$(l_1 m_1 l_2 m_2 | l_3 m_3) = (-1)^{l_2 - m_2} [(2l_3 + 1)(2l_1 + 1)]^{1/2} (l_2 - m_2 l_3 m_3 | l_1 m_1); \quad \text{(A9)}$$

$$\sum_{m_1} (l_1 m_1 l_2 m_2 | l_3 m)(l_1 m_1 l_2 m_2 | l_3' m) = \delta_{l_3 l_3'}; \quad \text{(A10)}$$

$$\sum_{l_3} (l_1 m_1 l_2 m_2 | l_3 m)(l_1 m_1' l_2 m_2' | l_3 m) = \delta_{m_1 m_1'}; \quad \text{(A11)}$$

and also satisfy the recoupling relation[20,28]

$$(l_3 m_3 l_2 m_2 | l_i m_i)(l_i m_i l_1 m_1 | lm) = \sum_{l_i'} (l_2 m_2 l_1 m_1 | l_{i'} m_{i'})(l_3 m_3 l_{i'} m_{i'} | lm) [l_3, (l_2 l_1) l_{i'}, l | (l_3 l_2) l_i, l_1, l], \quad \text{(A12)}$$

where $[l_3, (l_2 l_1) l_i', l | (l_3 l_2) l_i, l_1, l]$ is the Wigner recoupling coefficient (related to a 6-j symbol) and is independent of all m values. In (A5), $(\vec{E}^3)^{(l_i, l)}$ represents the m components of a degree l, order $(2l+1)$ irreducible standard set. Multiple occurrences of the degree l irreducible standard set are distinguished by the value of l_i. From (A6), l_i may be zero, one, or two, while l may equal three (when l_i is two), two (when l_i is either two or one), one(when l_i is either two, one, or zero), or zero (when l_i is one). The 27 elements of the triple vector product, after reduction via (A5), are the seven elements ($m = -l, -l+1, \ldots, +l$) of the irreducible set $(\vec{E}^3)^{(2,3)}$, five elements each of the

sets $(\vec{E}^3)^{(2,2)}$ and $(\vec{E}^3)^{(1,2)}$, three elements from each of the three sets $(\vec{E}^3)^{(2,1)}$, $(\vec{E}^3)^{(1,1)}$, and $(\vec{E}^3)^{(0,1)}$ and the lone element of the set $(\vec{E}^3)^{(1,0)}$. As in (A1), the ordering of the product $\vec{E}_1\times\vec{E}_2\times\vec{E}_3$ as it appears in (A5) is specific and permutation of the factors is not permitted. In anticipation of removal of the distinction between some or all of the applied fields, consider now the behavior of the various elements $(E^3)_m^{(l_i,l)}$ if such permutations were performed. Using (A7), interchange of $\vec{E}_2$ with $\vec{E}_3$ on the right-hand side of (A5) is seen to be equivalent to multiplication by $(-1)^{li}$, since $l_2 = l_3 = 1$. Hence for all allowed l and m, $(E^3)_m^{(li,l)}$ will be symmetric in E_2 and E_3 when l_i is 0 or 2, and antisymmetric when l_i is 1. Using the recoupling relation (A12), Eq. (A5) may be written

$$(E^3)_m^{(l_i,l)} = \sum_{m_1m_2m_3l_i'} (l_2m_2l_1m_1|l_{i'}m_{i'}) \times(l_3m_3l_{i'}m_{i'}|lm)(l_3,(l_2l_1)l_{i'},l| \times(l_3l_2)l_i,l_1,l)E_{1m_1}^{(l_1)}E_{2m_2}^{(l_2)}E_{3m_3}^{(l_3)}. \tag{A13}$$

The behavior of the right-hand side of (A13) upon interchange of $\vec{E}_2$ and $\vec{E}_1$ is seen to depend upon the values of l_i' as above, and also upon the recoupling coefficient. Since for completeness all recoupling coefficients are nonzero, the general element $(E^3)_m^{(l_i,l)}$ will have undefined or mixed symmetry under such interchange. However, three special cases exist. For l to equal 3, both l_i and l_i' must be 2; thus $(\vec{E}^3)^{(2,3)}$ will be symmetric on interchange of $\vec{E}_2$ with $\vec{E}_1$ as well as with $\vec{E}_3$. Similarly, when $l=0$, l_i and l_i' must be 1, and $(\vec{E}^3)^{(1,0)}$ is totally antisymmetric. A third special case arises when l is 1. Here, the two sets $(\vec{E}^3)^{(2,1)}$ and $(\vec{E}^3)^{(0,1)}$ are both symmetric in $\vec{E}_2$ and $\vec{E}_3$, and of these two sets a linear combination may be formed whose recoupling coefficient having l_i' equal to 1 vanishes. This combination also will be totally symmetric.

From these observations, it is apparent that a unitary transformation exists, connecting the sets $(\vec{E}^3)^{(li,l)}$ to the irreducible standard sets $(\vec{E}^3)^{(\nu,l)}$ (where ν specifies the symmetry of the set under the two interchange operations just discussed), and that ν will assume these values: ss_i, signifying a totally symmetric set; aa_i, signifying a totally antisymmetric set; ma_i, signifying a set symmetric in $\vec{E}_2$ and $\vec{E}_3$ but of mixed symmetry in $\vec{E}_1$ and $\vec{E}_2$; and ma_i, signifying a set antisymmetric in $\vec{E}_2$ and $\vec{E}_3$ and mixed in $\vec{E}_1$ and $\vec{E}_2$. Thus

$$(E^3)_m^{(\nu,l)} = \sum_{l_i} U_{\nu l_i}^{\ l}(E^3)_m^{(l_i,l)}, \tag{A14}$$

where the unitary matrix $U_{\nu l_i}^{\ l}$ is given in Table III.

The preceding development exactly parallels that by which the product-state wave function for three spin-1 particles is formed. That problem, for an arbitrary number of particles of arbitrary spin, has received much attention and becomes routine with the aid of Young's Tableaux,[56] neumonics which permit species determination by inspection, and Yahn's coefficients of fractional parentage[56] (our $U_{\nu l_i}^{\ l}$). Reference (57) consists of a set of reprints and an extensive bibliography in this field.

The response of the medium may now be specified by the 27 constants of proportionality between W, the interaction energy, and the 27 elements $(E^3)_m^{(\nu,l)}$, i.e., by the contrastandard set $\beta_m^{[\nu,l]}$ defined by the inner product relation

$$W = -\frac{1}{3}\left(\frac{n^2+2}{3}\right)^3 \sum_{\nu lm} \beta_m^{[\nu,l]}(E^3)_m^{(\nu,l)}. \tag{A15}$$

Using (A1), (A3), (A5), (A14), and (A15) we obtain

$$\beta_{ijk} = \sum_{\substack{\nu l l_i \\ m_1m_2m_3}} \beta_m^{[\nu,l]} U_{\nu l_i}^{\ l}(l_3m_3l_2m_2|l_im_i) \times(l_im_il_1m_1|lm)(l_im_i|i)(l_2m_2|j)(l_3m_3|k) = \sum_{\nu lm} \beta_m^{[\nu,l]} c_{ijk}^{\nu lm}, \tag{A16}$$

whence

$$c_{ijk}^{\nu lm} = \sum_{l_im_1m_2m_3} U_{\nu l_i}^{\ l}(l_3m_3l_2m_2|l_im_i) \times(l_im_il_1m_1|lm)(l_1m_1|i)(l_2m_2|j)(l_3m_3|k). \tag{A17}$$

Having employed unitary transforms at each step, $\vec{c}^{-1} = \vec{c}\,\dagger$, i.e.,

$$\beta_m^{[\nu,l]} = \sum_{ijk} c_{ijk}^{\nu lm*}\beta_{ijk} = \sum_{\substack{ijk \\ l_im_1m_2m_3}} U_{\nu l_i}^{\ l}(l_3m_3l_2m_2|l_im_i) \times(l_im_il_1m_1|lm)(l_1m_1|i)^*(l_2m_2|j)^* \times(l_3m_3|k)^*\beta_{ijk}. \tag{A18}$$

TABLE III. Elements of the unitary tensor $U_{\nu l i}^{\ l}$.

l	i_i	ν	ss_1	ms_1	ss_3	ms_2	ma_2	ma_1	aa
1	2		$(4/9)^{1/2}$	$-(5/9)^{1/2}$	0	0	0	0	0
1	0		$(5/9)^{1/2}$	$(4/9)^{1/2}$	0	0	0	0	0
3	2		0	0	1	0	0	0	0
2	2		0	0	0	1	0	0	0
2	1		0	0	0	0	1	0	0
1	1		0	0	0	0	0	1	0
0	1		0	0	0	0	0	0	1

The elements of $c_{ijk}^{\ \ \nu lm}$ have been evaluated using (A17) and appear as Table II.

While Eqs. (A17) and (A18) accomplish the objectives of the Appendix, several remarks are in order. First, consider the possibility of permuting the field amplitudes in (A5). For EHLS, two of the fields, say E_2 and E_3, derive from the same laser beam and are hence indistinguishable. Thus the sets $(\vec{E}^3)^{(\nu,l)}$, when ν implies antisymmetry in $\vec{E}_2$ and $\vec{E}_3$ will vanish, i.e., $(E^3)_m{}^{(ma_2,2)} = (E^3)_{m'}{}^{(ma_1,1)} = (E3)_0{}^{(aa,0)} = 0$ for all allowed m and m'. The corresponding coefficients $\beta^{[\nu,l]}$ need not be specified or alternatively may be set equal to zero. Thus, we obtain

$$\beta_m^{\ [ma_2,2]} = \beta_{m'}^{\ [ma_1,1]} = \beta_0^{\ [aa,0]} = 0 \ . \quad \text{(A19)}$$

Also, the distinction between the fields $\vec{E}_1$ and $\vec{E}_2$ lies solely in the difference in their frequencies. Permutations of $\vec{E}_1$ and $\vec{E}_2$ are thus forbidden only because of the dispersion in the nonlinear response of the medium.[58] Experimental attempts to detect effects due to this dispersion have all failed.[59] Thus in addition to (A19), coefficients $\vec{\beta}^{[\nu,l]}$ for $\nu = ms_i$, i.e., $\beta_m{}^{[ms_2,2]}$ and $\beta_{m'}{}^{[ms_1,1]}$ for all allowed m and m' will be small and to good approximation can be set equal to zero. In the limit of vanishing dispersion, the nonlinear response of the medium may be characterized either by the ten elements of a totally symmetric third-rank Cartesian tensor $\beta_{ijk} = \beta_{jki} = \beta_{kij} = \beta_{kji} = \beta_{jik} = \beta_{ikj}$ or by the elements of the two irreducible contra-standard sets $\vec{\beta}^{[ss_3,3]}$ (seven elements) and $\vec{\beta}^{[ss_1,1]}$ (three elements).

Next consider the transformation properties of $\vec{\beta}^{[\nu,l]}$ under coordinate rotations. If the reference frame is rotated by an amount specified by the Euler angle set $\{\psi,\theta,\varphi\} \equiv \vec{\Omega}$, a transformation is induced upon the elements of $\vec{\beta}^{[\nu,l]}$ as given by[28,28,55]

$$\beta_m^{\ [\nu,l]} = \sum_{m'} D_{mm'}^{[l]}(\vec{\Omega})\beta_{m'}^{\ [\nu,l]} \ , \quad \text{(A20)}$$

where $D_{mm'}{}^{(l)}(\vec{\Omega}) = D_{mm'}{}^{[l]*}(\vec{\Omega})$ are matrix elements of the finite rotation operator and are proportional to the symmetric top eigenfunctions. In the Cartesian representation, on the other hand, this transform is given by

$$\beta_{ijk} = \sum_{\alpha\beta\gamma} S_{i\alpha}(\vec{\Omega})S_{j\beta}(\vec{\Omega})S_{k\gamma}(\vec{\Omega})\beta_{\alpha\beta\gamma} \ , \quad \text{(A21)}$$

where $S_{ij}(\vec{\Omega})$ is the Cartesian rotation matrix.[8] In (A21) all elements of $\beta_{\alpha\beta\gamma}$ are intermixed, whereas in spherical representation only elements having the same l and ν are intermixed. In fact, the process of expressing β in terms of irreducible sets is equivalent to reducing the 27-dimensional representation of R_3 provided by $S_{i\alpha}(\vec{\Omega})S_{j\beta}(\vec{\Omega})S_{k\gamma}(\vec{\Omega})$ to irreducible form. Further, the $D_{mm'}{}^{(l)}(\vec{\Omega})$, as functions of $\vec{\Omega}$, satisfy the orthogonality conditions[20,28]

$$\int_0^{2\pi} d\psi \int_0^{2\pi} \sin\theta\, d\theta \int_0^{2\pi} d\varphi D_{mn}^{\ (l)}(\vec{\Omega})D_{m'n'}^{\ (l')}(\vec{\Omega}) = [8\pi^2/(2l+1)]\delta_{mm'}\delta_{nn'} \ ; \quad \text{(A22)}$$

obey the Schrödinger equation

$$\nabla_\Omega^2 D_{mm'}^{\ (l)}(\vec{\Omega}) = -l(l+1)D_{mm'}^{\ (l)}(\vec{\Omega}) \ , \quad \text{(A23)}$$

∇_Ω^2 being the Laplacian operator in Euler angle space; and further satisfy

$$D_{mk}^{\ (l)}(\vec{\Omega}_1 + \vec{\Omega}_2) = \sum_{m'=-l}^{l} D_{mm'}^{\ (l)}(\vec{\Omega}_1)D_{m'k}^{\ (l)}(\vec{\Omega}_2) \ ,$$

$$D_{00}^{\ (0)}(\vec{\Omega}) = 1, D_{mk}^{\ (l)*}(\vec{\Omega}) = (-1)^{m-k}D_{-m-k}^{\ (l)}(\vec{\Omega})$$

and $$D_{km}^{\ (l)}(-\vec{\Omega}) = D_{km}^{\ (l)*}(\vec{\Omega}) \ .$$

Since the transform matrix $D_{mm'}{}^{(l)}(\vec{\Omega})$ is unitary, the spaced-fixed nonlinearity tensor of a

molecule whose orientation is $\vec{\Omega}$ becomes

$$\beta_m^{[\nu,l]} = \sum_{m'} \bar{\beta}_{m'}^{[\nu,l]} D_{m',m}^{(l)}(\vec{\Omega}) \equiv \beta_m^{[\nu,l]}(\vec{\Omega}) . \tag{A24}$$

$\bar{\beta}[\nu,l]$, the molecule fixed nonlinearity tensor, must reflect the point symmetries of the molecule it characterizes, and hence many relations will exist among its various elements. The exact form of $\bar{\beta}$ as restricted by the various point groups can be found in the literature,[4] but only in Cartesian representation. Relation (A1) may then be used to determine the symmetry-restricted form of the sets $\bar{\bar{\beta}}[\nu,l]$.

Last, consider the transformation of the relation

$$p_{1_i} = \beta_{ijk} E_{2_j} E_{3_k} \tag{A25}$$

to spherical representation. As an alternative to (A15), W can be expressed as the inner product of the contrastandard set $p_{1m}{}^{l_1}$ with the standard set $E_{1_{m_1}}{}^{(l_1)}$, i.e.,

$$W = \sum_{m_1} p_{1_{m_1}}{}^{[l_1]} E_{1_{m_1}}{}^{(l_1)} = \sum_{\substack{l_i l \\ m_1 m_2 m_3 m}} \beta_m^{[l_i,l]} \times (l_3 m_3 l_2 m_2 | l_i m_i)(l_i m_i l_1 m_1 | lm) \times E_{1_{m_1}}{}^{(l_1)} E_{2_{m_2}}{}^{(l_2)} E_{3_{m_3}}{}^{(l_3)} . \tag{A26}$$

Thus $$p_{m_1}{}^{[l_1]} = \sum_{l l_i m_i m} \beta_m^{[l_i,l]} (l_i m_i l_1 m_1 | lm) \times (-1)^{l_i - m_i} (E^2)_{-m_i}^{[l_i]} , \tag{A27}$$

where $$(E^2)_{m_i}^{(l_i)} = \sum_{m_2 m_3} (l_3 m_3 l_2 m_2 | l_i m_i) \times E_{2_{m_2}}^{(l_2)} E_{3_{m_3}}^{(l_3)} , \tag{A28}$$

and the transformation to a contrastandard set $(\vec{E}^2)^{[li]}$ is accomplished via the relation[55]

$$(E^2)_{m_i}^{(l_i)} = \sum_{m_i'} U_{m_i m_i'}^{[l_i]} \times (E^2)_{m_i'}^{[l_i]} = (-)^{l_i - m_i} i (E^2)_{-m_i}^{[l_i]} . \tag{A29}$$

Using (A8), (A27) may be rewritten

$$p_{m_1}{}^{[l_1]} = \sum_{l l_i m_i} \left(\frac{2l+1}{2l_1+1} \right)^{1/2} (l_m l_i m_i | l_1 m_1) \times \beta_m^{[l_i,l]} (E^2)_{m_i}^{[l_i]} . \tag{A30}$$

Thus $p_{m_1}[l_1]$ does *not* correspond to the irreducible contrastandard set of degree 1 resulting from the product of $\beta_m^{[l_i,l]}$ with $(E^2)_{m_i}^{[li]}$. This seeming inconsistency may be traced to the fact that the interaction energy is the *inner product* of $p_{1_{m_1}}{}^{[l_1]}$ with $E_{1_{m_1}}{}^{(l_1)}$ or of $\beta_m^{[l_i,l]}$ with $(E^3)_m^{(l_i,l)}$, and not as the corresponding *product of degree zero.*

[1] R. W. Terhune, P. D. Maker, and C. M. Savage, Phys. Rev. Letters 14, 681 (1965).

[2] Y. Y. Li, Acta Phys. Sinica 20, 164 (1964).

[3] J. C. Decius and J. E. Rauch, Ohio State Symposium of Molecular Structure and Spectroscopy Report No. 48, 1959 (unpublished).

[4] S. J. Cyvin, J. E. Rauch, and J. C. Decius, J. Chem. Phys. 43, 4083 (1965).

[5] S. Kieleich, Bull. Acad. Polon. Sci. 12, 53 (1964); Acta Phys. Polon. 33, 89 (1968).

[6] R. Bershon, Y. H. Pao, and H. L. Frisch, J. Chem. Phys. 45, 3184 (1966); Y. H. Pao, H. L. Frisch, and R. Bershon, Intern. J. Quantum Chem. 1S, 829 (1967).

[7] D. L. Weinberg, J. Chem. Phys. 47, 1307 (1967).

[8] H. Goldstein, Classical Mechanics (Addison-Wesley Publishing Co., Inc., Reading, Mass., 1950).

[9] A. D. Buckingham and B. J. Orr, Quart. Rev. 21, 195 (1967).

[10] A. D. McLean and M. Yoshimine, J. Chem. Phys. 46, 3682 (1967).

[11] V. S. Starnov, Opt. Spektry. (USSR) 18, 300 (1965) [English transl.: Opt. i Spectroskopiya 18, 165 (1965)] and papers cited.

[12] D. A. Pinnow, S. J. Candau, and T. A. Litovitz, J. Chem. Phys. 49, 347 (1968).

[13] R. Pecora, J. Chem. Phys. 49, 1032 (1968); 49, 1036 (1968); W. A. Steele and R. Pecora, *ibid.* 42, 1863 (1965); 42, 1872 (1965).

[14]W. A. Steele, J. Chem. Phys. 38, 2404 (1963).
[15]R. G. Gordan, J. Chem. Phys. 43, 1307 (1965); and earlier papers.
[16]L. D. Landau and E. M. Lifshitz, Electrodynamics of Continuous Media (Addison-Wesley Publishing Co., Inc., Reading, Mass., 1960), p. 377.
[17]M. C. Wang and G. E. Uhlenbeck, Rev. Mod. Phys. 17, 323 (1945).
[18]See, for instance, N. Davidson, Statistical Mechanics (McGraw-Hill Book Co., New York, 1962).
[19]L. van Hove, Phys. Rev. 95, 249 (1954).
[20]M. E. Rose, Elementary Theory of Angular Momentum (John Wiley & Sons, Inc., New York, 1957).
[21]R. H. Cole, J. Chem. Phys. 42, 637 (1965).
[22]T. A. Litovitz and G. McDuffie, J. Chem. Phys. 39, 729 (1963).
[23]N. Bloembergen, E. M. Purcell, and R. V. Pound, Phys. Rev. 73, 679 (1948).
[24]A. Abragam, The Principles of Nuclear Magnetism (Oxford University Press, Oxford, 1961).
[25]E. N. Ivanov, Zh. Eksperim. i Teor. Fiz. 45, 1509 (1963) [English transl.: Soviet Phys. – JETP 18, 1041 (1964)].
[26]L. D. Favro, Phys. Rev. 119, 53 (1960).
[27]K. A. Valiev and L. D. Eskin, Opt. i Spectroskopiya 12, 429 (1962) [English transl.: Opt. Spectry (USSR) 12, 758 (1962)]; *ibid* 13, 282 (1962) [13, 505 (1962)].
[28]A. R. Edmonds, Angular Momentum in Quantum Mechanics (Princeton University Press, Princeton, N.J., 1957).
[29]A. S. Pine, Phys. Rev. 149, 113 (1966); R. Chiao, C. H. Townes, and R. Stoicheff, Phys. Rev. Letters 12, 592 (1964).
[30]J. A. Saxton, Proc. Roy. Soc. (London) A213, 473 (1952).
[31]S. J. Bass, W. I. Nathan, R. M. Meighan, and R. H. Cole, J. Phys. Chem. 68, 509 (1964).
[32]H. S. Gabelnick and H. L. Strauss, J. Chem. Phys. 49, 2334 (1968); 46, 396 (1967).
[33]G. I. Zaitser and V. S. Starnov, Opt. i Spectroskopiya 19, 497 (1965) [English transl.: Opt. Spectry (USSR) 19, 847 (1965)].
[34]A. A. Anthony and C. P. Smyth, J. Am. Chem. Soc. 86, 152 (1964).
[35]Krishnaji and A. Mansingh, J. Chem. Phys. 41, 827 (1964).
[36]G. B. Rathman, A. J. Curtis, P. L. McGreer, and C. P. Smyth, J. Chem. Phys. 25, 413 (1956).
[37]V. Sarojini, Trans. Faraday Soc. 58, 1729 (1962).
[38]D. J. Denney and J. W. Ring, J. Chem. Phys. 39, 1268 (1963).
[39]G. E. McDuffie and M. V. Kelley, J. Chem. Phys. 41, 2666 (1964).
[40]A. D. Buckingham and J. A. Pople, Proc. Phys. Soc. (London) A68, 905 (1955).
[41]N. Bloembergen and P. Lallemand, Phys. Rev. Letters 16, 81 (1966).
[42]R. W. Hellwarth, Phys. Rev. 152, 156 (1966).
[43]K. R. Symon, Mechanics (Addison-Wesley Publishing Co., Inc., Reading, Mass., 1960).
[44]N. Bloembergen, Am. J. Phys. 35, 989 (1967).
[45]C. C. Wang, Phys. Rev. 152, 149 (1966); C. A. Sacchi, C. H. Townes, and J. R. Lifsitz, *ibid.* 174, 439 (1968).
[46]C. C. Wang, Phys. Rev. Letters 14, 344 (1966).
[47]S. H. Glarum, J. Chem. Phys. 33, 1371 (1960).
[48]J. A. Glasel, Proc. Nat. Acad. Sci. 58, 27 (1967).
[49]P. D. Maker, in Physics of Quantum Electronics, edited by P. L. Kelley, B. Lax, and P. E. Tannenwald (McGraw-Hill Book Co., New York, 1966), p. 60.
[50]R. E. Nettleton, J. Acoust. Soc. Am. 31, 557 (1959).
[51]H. B. Levine and G. Birnbaum, Phys. Rev. Letters 20, 439 (1968).
[52]E. E. Bray and N. S. Gingrich, J. Chem. Phys. 11, 351 (1943).
[53]R. W. Gruebel and G. T. Clayton, J. Chem. Phys. 46, 639 (1967).
[54]A. H. Narten, M. D. Danford, and H. A. Levy, J. Chem. Phys. 46, 4857 (1967).
[55]U. Fano and G. Racah, Irreducible Tensorial Sets (Academic Press Inc., New York, 1959).
[56]H. A. Jahn and H. van Wieringen, Proc. Roy. Soc. (London) A209, 502 (1951).
[57]Quantum Theory of Angular Momentum edited by L. C. Biedenharn and H. Van Dam (Academic Press Inc., New York, 1965).
[58]D. A. Klienman, Phys. Rev. 126, 1977 (1962); P. S. Pershan, *ibid.* 130, 919 (1963).
[59]R. C. Miller, Appl. Phys. Letters 5, 17 (1964); R. C. Miller, D. A. Klienman, and A. Savage, Phys. Rev. Letters 11, 146 (1963).